

Theory of multiple phase separations in binary mixtures: Phase diagrams, thermodynamic properties, and comparisons with experiments

Raymond E. Goldstein

Departments of Chemistry and Physics, Massachusetts Institute of Technology, Cambridge, Massachusetts 02139

James S. Walker^{a)}

Department of Physics, Massachusetts Institute of Technology, Cambridge, Massachusetts 02139
(Received 13 August 1982; accepted 21 October 1982)

The lattice-gas models of phase separating binary liquid mixtures, introduced by Walker and Vause, are studied in detail and generalized within a high-temperature series expansion. This approximation allows for a straightforward study of rather complex, orientationally specific pair interactions, like those found in real systems. These theories can predict much of the complex miscibility phenomena often found in these mixtures, which are characterized by hydrogen-bonding interactions. Such phenomena include up to five critical solution points as a function of temperature. By comparisons with experiments, we determine the model parameters, thus mapping these experiments onto the global phase diagrams. These experiments include studies of the dependence of liquid/liquid miscibility on temperature, pressure, concentration of electrolytes, and addition of a dilute third component. Specifically, we make direct comparison with various experiments on the binary systems 2-butanol + H₂O, 3-methyl pyridine + H₂O(D₂O), glycerol + *o*-methoxy phenol and ethanol + H₂O + electrolytes. Very simple and often easily interpreted trends in the parameters are found and quantitative agreement with experiments is possible with minimum parametric freedom. Explicit predictions of critical exponent renormalization in several systems are made. In addition, suggestions are made for a number of light scattering and specific heat experiments, some of which may demonstrate incipient critical behavior, such as the onset of long range correlations, in systems not undergoing phase separation.

I. INTRODUCTION

The properties of binary liquid mixtures are of interest to condensed-matter theorists, experimental chemists and physicists, and the chemical industry, among others.¹⁻⁴ An understanding of the intermolecular forces which give rise to the diverse phenomena observed experimentally is important for both very practical, applications-oriented reasons and to test theories of phase transitions and critical phenomena.^{3,4} Such experiments can involve variations in temperature or pressure, addition of electrolytes or a dilute third component, isotope substitution, etc. In this paper, we explore, in depth, lattice-gas models of mixtures of strongly interacting organic liquids, introduced by Walker and Vause.⁵⁻⁷ Our results are related to theoretical and experimental work: (1) We study several model Hamiltonians which we believe embody the essential physics underlying these complex systems. This is accomplished by the application of a simple approximation technique⁸ which allows for a straightforward study of very specific interparticle interactions, such as those which appear to be present in these mixtures. (2) We show that a wide range of phase transition experiments can be located on the global phase diagrams of these simple models, and we develop methods for implementing these "mappings." Furthermore, explicit predictions about various thermodynamic properties of several systems are made along with suggestions for appropriate experiments.

^{a)}Present address: Department of Chemistry, B-014, University of California, La Jolla, CA 92093.

A. Background

Many binary liquid mixtures which form a single, homogeneous phase at high temperatures possess an upper critical solution temperature (UCST) below which phase separation occurs.² In simple systems of structureless particles, such as rare gas binary mixtures, the existence and specific value of an UCST are consequences of the energetics of interparticle interactions balanced against the entropy of mixing. The properties of more complex mixtures, such as aliphatic and aromatic alcohols, ketones, amines, and ethers in solution with water or alcohols, can only be understood through consideration of configurational entropy, as well as energetics. For such systems, realistic theoretical descriptions recognize the fact, pointed out by Hirschfelder, Stevenson, and Eyring,⁹ that highly directionally specific, yet weak interparticle attractive forces (such as hydrogen bonds and dipolar forces) can produce the reentrance of a mixed homogeneous phase at low temperatures. This produces a "closed-loop" temperature-composition ($T-x$) phase diagram and an associated lower critical solution temperature (LCST), below which a single homogeneous phase exists. The predominant low temperature species is then a bound A-B pair (in a mixture of A and B molecules) with many rotational degrees of freedom effectively "frozen out" by the bonding. Hence, this phase is actually characterized by less entropy than the higher temperature separated phases (in accord with the third law), although it appears more random because it is mixed. Of course, this phenomenon of bonding need not be accompanied by an intermediate miscibility gap, depending upon the balance of energy

of bonding, entropy of mixing, etc. Furthermore, a freezing transition may preempt the reentrance of a homogeneous phase.

The above miscibility/immiscibility behavior is most typically seen with temperature as the variable thermodynamic field, although many other degrees of freedom can be explored. For example, pressure (P) variation has been extensively studied, especially in mixtures of substituted pyridines and water.¹⁰⁻¹² The fundamental phenomenon in such systems is an immiscibility "dome" in T - P - x space, with the apex of the dome at high pressures and complete miscibility at higher pressures. Variation in miscibility gaps can also be accomplished by the introduction of electrolytes of various types into these solutions,^{13,14} or the substitution of D_2O for normal water as the solvent.¹⁵ By introducing these extra thermodynamic degrees of freedom, critical point properties can be studied in detail: Critical loci can be expanded in dimensionality and critical exponent scaling,¹⁶ universality,¹⁷ and renormalization^{17,18} (e.g., accompanying the merging of two or more critical points) can be studied conveniently.

Many detailed studies of the critical-point properties of these systems have confirmed Ising-like behavior⁴ for the temperature (or pressure) dependence of the order parameter (suitably defined) as well as the amplitude ratio and exponent of the specific heat anomaly¹⁹ at each of the critical temperatures.

B. Theoretical models and methods

The successful theories of binary mixture behavior include both continuum^{20,21} and lattice-gas models. We discuss only the latter here. The Ising model can be formulated to describe a binary mixture through the standard correspondence involving nearest-neighbor (nn) pair interaction energies.³ This approach will not predict lower critical solution temperatures if the energies are taken to be temperature independent (see Sec. II A). The efforts toward understanding entropic effects include the original Barker-Fock model²² and the more recent and successful decorated lattice theories of Wheeler and co-workers.²³⁻²⁶ A common feature of these models is the singling out of a small subset of the many orientational states of a nearest-neighbor pair of particles as energetically more favorable than the others. The directional specificity is then controlled by the size of that subset relative to the total number of orientational configurations. Such models generate temperature-dependent coupling constants, thus allowing for closed-loop phase diagrams. A disadvantage of the decorated lattice models is that they do not treat all lattice sites equivalently. As a result, bonding interactions cannot propagate throughout the entire lattice, whereas the real systems have no such restriction.

Renormalization-group (RG) calculations, especially involving position-space RG (PSRG) techniques (e.g., of the Migdal-Kadanoff^{27,28} type) are attractive because they allow for the explicit formulation of a many-particle Hamiltonian for which all lattice sites are equivalent and bonding interactions can propagate to arbitrary lengths. The models of Walker and Vause⁵⁻⁸ (WV) are easily

treated with PSRG methods and achieve quite good agreement with experiments. The global phase diagrams of these models allow for a rich variety of phenomena from simple phase separation to closed-loop diagrams, "freezing" transitions and critical double points.

Both the decorated lattice models^{24,25} and those studied here have recently been extended by including the interactions between like molecules in addition to the unlike-molecule hydrogen-bonding forces.^{6,7} Thus, a whole new range of phenomena has been encompassed, including the possibility of three critical points as a function of temperature, as seen in many real systems.

C. Outline of paper

In Sec. II of this paper we review the WV models and present the physical motivations for the Hamiltonians. Also discussed is a simple re-derivation of the lowest order results of a high-temperature series expansion introduced elsewhere.⁸ We explore the qualitative features of the resultant global phase diagrams along with presenting expressions for many of the important thermodynamic properties (entropy, specific heat, nearest-neighbor correlations, etc.). Section III is devoted to the explicit comparison of these models to a wide variety of phase transition experiments. Simple methods are developed for the fitting of solubility and other experimental data with the parameters of these models. In some cases, simple physical/chemical explanations of the observed trends are proposed. Also covered are several extensions of the models to very complex systems. Section IV is a summary of the work.

II. THEORETICAL ASPECTS

A. Models and calculational methods

We begin this section by describing the WV models. These have been studied using RG methods,^{5-7,29,30} as well as a recently introduced technique in which a subset of the total degrees of freedom is traced out of the system.⁸ We re-derive this "trace-out" method (as it will be referred to in this paper) in a very simple way, and apply it to an extended version of the original model. In the second part of this section we develop relations for various thermodynamic quantities, such as the entropy, nearest-neighbor correlations and specific heat, and we study these basic quantities as illustrative of the processes inherent in these mixtures.

As described in the Introduction, the phenomenon of phase separation in binary liquid mixtures can generally be described as an Ising-like transition. While measurements of critical exponents verify that such systems are in the Ising universality class, simple considerations of symmetry properties also lead to this conclusion.³ In the simplest cases, then, one can study such mixtures in terms of the basic Ising model, which can be written as

$$-\beta\mathcal{H} = \sum_{\langle ij \rangle} K(1 - \delta_{s_i s_j}) \quad (1)$$

where $\sum_{\langle ij \rangle}$ is a sum over nearest-neighbors on the lat-

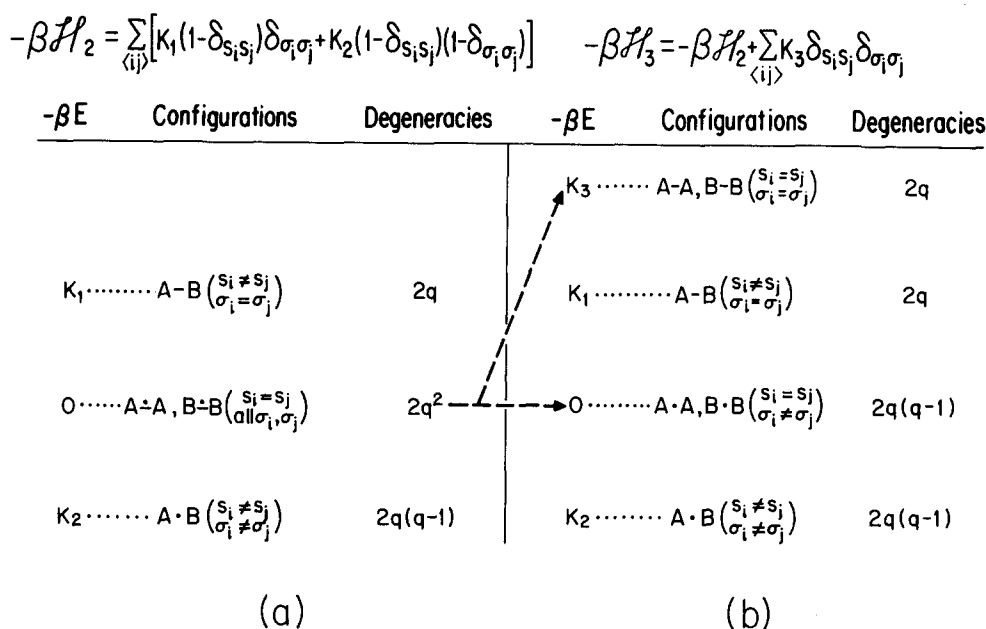


FIG. 1. Descriptions of (a) two-, (b) three-parameter lattice-gas Hamiltonians for binary fluid mixtures. The sums are over nearest-neighbor pairs on a hypercubic lattice. Ising variables ($s_i = A, B$) refer to molecular identity while Potts variables ($\sigma_i = 1, 2, 3, \dots, q$) refer to molecular orientation. The energy level hierarchy in (a) is appropriate for closed-loop phase diagrams, while (b) describes a system with a phase separated ground state.

tice, $\beta = 1/k_B T$, $s_i = A, B$ (representing the two types of molecules in the mixture), and $\delta_{s_i s_j}$ is the Kronecker delta function. This Hamiltonian produces two energy levels; K , if nearest-neighbor molecules are unlike (AB), and zero if the molecules are of the same type (AA or BB). Since K is defined to be $-\beta$ times an energy, it follows that when $K < 0$ configurations describing phase separation AA and BB are energetically favored relative to the mixed state AB, and therefore are favored at low temperatures. However, the mixed state is favored entropically, and thus will predominate at high temperatures. As a result, at some intermediate temperature the system will change from one state to the other by way of an Ising critical transition.

This model predicts that the phase separation persists for all temperatures lower than the upper critical solution temperature (UCST). It will not describe the appearance of a lower critical solution temperature (LCST). As explained in the introduction, the reappearance of the mixed phase at lower temperatures is intimately related to additional degrees of freedom in the system, such as molecular orientation, and the couplings between the various degrees of freedom. In particular, we are primarily interested in systems in which hydrogen bonding between the components of the mixture is important. To describe the bonding interactions we need to introduce an additional degree of freedom accounting for the molecular orientations, and to describe their interactions.

Consider, in addition to the Ising variables $s_i = A, B$, another variable $\sigma_i = 1, 2, 3, \dots, q$, which describes the orientation of each molecule. We choose the orientational degrees of freedom to be discrete for simplicity. As we shall see below, it is possible to consider continuous variables as well, however, the basic qualitative fea-

tures of interest are embodied in this discrete formulation. We imagine, then, that each molecule can point in one of q directions, i. e., the total solid angle associated with each molecule is divided into q sections, each describing roughly the solid angle of the bonding element. These variables are then coupled via the two-parameter Hamiltonian,

$$-\beta\mathcal{H}_2(K_1, K_2) = \sum_{\langle ij \rangle} [K_1(1 - \delta_{s_i s_j}) \delta_{\sigma_i \sigma_j} + K_2(1 - \delta_{s_i s_j})(1 - \delta_{\sigma_i \sigma_j})]. \quad (2)$$

The energy levels and their degeneracies are shown in Fig. 1(a).

We can best describe the features of the model by considering each of the energy levels in turn. First, if nearest-neighbor molecules are of the same type, then $(1 - \delta_{s_i s_j}) = 0$, and this configuration defines for us the zero of energy. If adjacent lattice sites are occupied by molecules of different types, then two energies can result, depending on the values of σ_i, σ_j ; i. e., depending on the orientational states of the molecules. This discrete model describes bonding very simply by saying that unlike molecules either bond or do not bond. If they bond we represent this by saying that $\sigma_i = \sigma_j$. By this we do not mean that the molecules point in the same direction in space, but rather, that their relative orientations are correct for bonding to occur. Thus, all bonding configurations are collected in the $\sigma_i = \sigma_j$ state with favorable reduced energy $K_1 > 0$. If the relative orientation is not appropriate for bonding, represented by $\sigma_i \neq \sigma_j$, then the system suffers the repulsive energy $K_2 < 0$. In Fig. 1(a) we represent bonding by $-$ and non-bonding by $\cdot\cdot$. At this point, we do not consider bonding between like molecules, but we shall return to this feature shortly.

The model now has the basic energy levels to represent

the systems of interest, but equally important is the degeneracy structure of these levels, also displayed in Fig. 1(a). In the bonding state K_1 , the σ_i 's can satisfy the condition $\delta_{\sigma_i \sigma_j} = 1$ in q different ways, and thus this level has a degeneracy of $2q$. The factor of 2 comes from counting A-B and B-A configurations. Nonbonding occurs much more often than bonding, however, and more so the more directionally specific is the interaction (i. e., the larger q becomes). In this model the nonbonding state K_2 has a degeneracy $2q(q-1)$; greater than that for bonding by roughly a factor of q for the large q used here (~ 500). Like molecules do not bond in this model, and thus they are free to take on any orientation, giving rise to a degeneracy of $2q^2$, again up by a factor of q . Therefore, even though the level K_1 is energetically most favorable, it is also entropically disfavored. In fact, since the degeneracy associated with K_1 is down by a factor of q , this level will not be important in the system, because of entropy considerations, until the temperature is lowered to the order of $1/\ln q$ (in reduced units).

We can now understand the basic workings of the model. At high temperatures only the energy levels 0 and K_2 are important in the system, because of their large degeneracies. These energy levels are essentially what one would obtain for the Ising model [Eq. (1)] and thus will tend to produce an UCST. As the temperature is lowered to $\sim 1/\ln q$, the bonding level K_1 now becomes important, and the system seeks to mix again so that the favorable A-B bonding can take place. This produces the LCST. Similarly, we see that even though the mixing entropy increases as the temperature is lowered, much more entropy is lost by falling into the bonding level with its low orientational entropy. The result is that the total entropy monotonically decreases, as required by thermodynamics. Finally, if the bonding level is too favorable energetically, it can overcome its entropic disadvantage, and the system may never separate at all.

Several studies⁵⁻⁸ have shown this model to be quite accurate, quantitatively as well as qualitatively. Perhaps its most accurate solution to date results from the PSRG method of Migdal and Kadanoff^{27,28} (MK) and these calculations have been presented in detail elsewhere.⁵⁻⁷ Here, we shall recall some of the major findings of the PSRG studies, and use them to motivate and illustrate the simple calculational method which we use in this paper. In Fig. 2, the phase diagram obtained within the Migdal-Kadanoff approximation is plotted in interaction-parameter space (K_1, K_2) for negative K_2 , with $q = 500$. First, note that when $K_1 = K_2$, the bonding and nonbonding energies are the same, thus bonding no longer plays a role and the model reduces to the Ising model. This is of particular importance because of the wealth of information available for the Ising model.^{3,31-33} In the MK calculation the critical point is represented by the fixed point of the RG "flow," located at point F. For $|K_1| = |K_2|$ less than the critical value, the system is mixed, in a more or less random manner, while for $|K_1| = |K_2|$ greater than this value the system is phase separated. The curve XY in Fig. 2 separates these two phases, and every point on this curve is itself an Ising

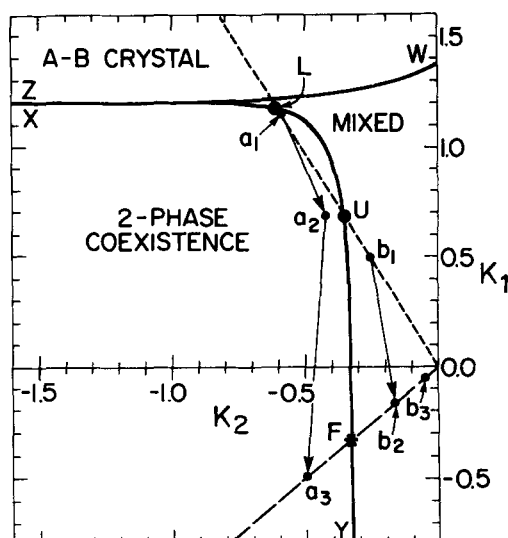


FIG. 2. Quadrant II of the global phase diagram for the two-parameter Hamiltonian (Eq. (2)) with $q=500$, obtained from a Migdal-Kadanoff position-space renormalization group calculation (Ref. 5). The locus of initial conditions for a given system extends from the origin through points U and L, the UCST and LCST, respectively. Point F is the Ising subspace fixed point of the MK recursions. Points a_1 - a_3 and b_1 - b_3 show typical RG flows, demonstrating the rapid convergence to the Ising subspace (the line $K_1 = K_2$).

critical point. When $K_1 \rightarrow +\infty$ and $K_2 \rightarrow -\infty$ the system settles into a ground state of alternating A and B molecules which are all bonded to one another, in other words, a crystal. The curve ZW separates the mixed phase from the crystal phase. It should be noted that there is always a thin wedge of the mixed phase between the curves XY and ZW, so that these curves never actually touch. That is, freezing never preempts the LCST in this model.

Now, the interpretation of this phase diagram in terms of a physical system is as follows: Any given mixture of molecules will have a representative bonding energy $J_1 = -K_1/\beta (< 0)$ and nonbonding energy $J_2 = -K_2/\beta (> 0)$. These energies are givens of the molecular system, and thus a mixture can be characterized by its value of $R = -K_1/K_2$ (and also q). The initial conditions of the system thus lie along a ray extending from the origin, as indicated by the dashed line in Fig. 2, with temperature (T) becoming lower with increasing distance from the origin. Thus, at high T the system is mixed. As temperature is lowered an UCST is encountered at the point U, and lower in T the LCST is encountered at L. Below this the system is mixed again, and finally, at still lower temperatures, it will freeze. Thus, we see that closed-loop phase diagrams are indeed produced.

It is interesting to note that under the PSRG mappings, the initial system rapidly flows, or renormalizes, to a simple Ising model. For example, if the initial condition is point a_1 (Fig. 2), then after one renormalization, the system flows to point a_2 . With one more renormalization the system is essentially an Ising model at point a_3 , since $K_1 \approx K_2$. Similarly, starting at point b_1 the system again flows under two RG iterations to approach

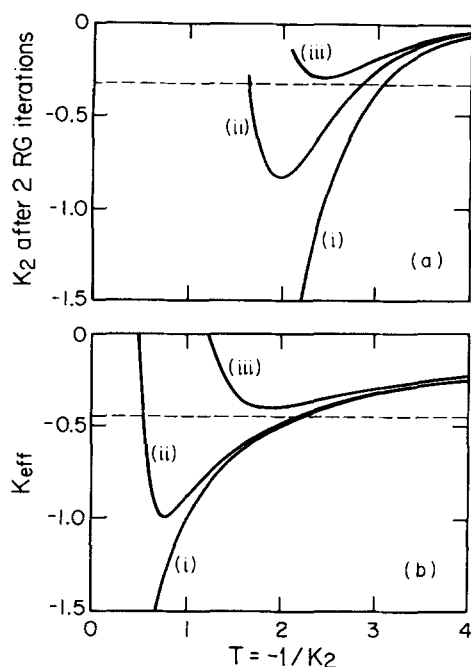


FIG. 3. Coupling constants as a function of temperature for the two-parameter model [Eq. (2)] with $q=500$. Note that this coupling is for an Ising model written as in Eq. (1). (a) K_2 after two iterations of the MK recursion relations, for temperatures above the freezing transition. Curves (i) through (iii) are for $R (= -K_1/K_2)$ of $-1, 1.95, 3.7$, respectively. (b) Results of the trace-out method showing the same qualitative behavior. $R = -1, 3, 7$ for curves (i), (ii), and (iii). In (b) the dashed line is at the critical value of the coupling constant for the 3-d Ising model, while in (a) it is at the value found in the MK approximation (see Ref. 5).

a simple Ising model at point b_3 . Thus, the RG calculation in effect tells us that after a few renormalizations the σ variables (orientational degrees of freedom) no longer have an effect, but rather the system is now an Ising model whose temperature dependence is rather interesting. In Fig. 3(a) we illustrate this by plotting K_2 after two RG iterations vs the initial temperature. Note that we have chosen the Kronecker delta notation in Eq. (2) and the Ising coupling constants are < 0 for ferromagnetic (AA, BB) ordering. This plot then shows the effective Ising coupling as a function of temperature. Case (i) is for $R = -1$, that is $K_1 = K_2$. In this case our model reduces to the Ising model and thus the strength of the coupling monotonically increases (i.e., becomes more negative) as temperature is lowered. The dashed line in Fig. 3(a) indicates the critical coupling, so that for $R = -1$ there is only one critical point, an UCST. For lower temperatures the system becomes increasingly separated. Case (ii) corresponds to a value of R , similar to that shown in Fig. 2, which produces a closed loop. As temperature is lowered the effective coupling crosses the critical value, producing an UCST. At still lower T the effective coupling rises, again crossing the critical value, producing a LCST, and the system becomes mixed. Finally, case (iii) illustrates the situation in which R is too large to produce a loop (miscibility gap). Thus, the effective coupling never crosses below

the dashed line, and therefore no phase separation occurs.

We obtain qualitatively the same results using a much simpler method, which can be thought of in the following way. The RG calculation has shown that after only a few renormalizations the σ variables are effectively taken out of the problem, so that the system maps to an Ising model. It has been shown that, within a high-temperature series expansion, one can trace out the σ variables in a single step, to a very good approximation, creating in the process an effective Ising coupling.⁸ In a sense, the σ variables are irrelevant in that they do not change the phase separation transition to a universality class other than that of the Ising model. Instead, the effect of the σ variables is simply to alter the way the coupling depends on temperature. This is illustrated in Fig. 3(b), where we plot the result (derived below)

$$K_{\text{eff}} = \frac{-1}{T} + \ln \left(1 + \frac{1}{q} \{ \exp[(R+1)/T] - 1 \} \right), \quad (3)$$

vs $T = -1/K_2$. Recall that this expression refers to the formulation in Eq. (2), and gives ferromagnetic ordering for $K_{\text{eff}} < K_{\text{critical}} < 0$. This expression for K_{eff} can be shown⁸ to be exact through order $(v/q)^3$, where

$$v = \exp[(R+1)/T] - 1. \quad (4)$$

Shortly, we shall re-derive this result in a more general context.

It is clear from Fig. 3(b) that the effective coupling generated by tracing out the σ variables has the same qualitative features as the RG transformation. We can translate Fig. 3(b) back into a phase diagram in interaction space (K_1, K_2) , as in Fig. 2, by recalling that each case shown in Fig. 3(b) corresponds to a given value of R , and thus for any ray extending from the origin we can determine the location of the critical points (if any). The result, shown in Fig. 4(a), is qualitatively very similar to the PSRG phase diagram in Fig. 2. Note that the transition from the mixed to crystal phase is an Ising anti-ferromagnetic transition in this trace-out method, while in the RG case it is a $2q$ -state Potts model³⁴ transition, which for large q is known to be first order,³⁵ as expected for freezing. Thus, the RG calculation is the more accurate of the two, though, as we shall see, the trace-out technique is very easy to use and is qualitatively correct for the phase separation transitions. Note that, while the freezing transition is in a different universality class, the ground state is the same—an A-B strongly bonded phase.

Figure 4(b) shows the T - x phase diagrams obtained from this simple calculation, where the two points plotted for temperatures within the loops are $x_{\pm} = \frac{1}{2}(1 \pm M)$, and M is the Ising spontaneous magnetization. The closed-loop phase diagrams have the correct qualitative features, such as a greater "flatness" near the bottom than near the top, though quantitatively we find that the loop is generally somewhat narrower than that of the more accurate RG calculation.

We now describe how to implement the trace-out method in practice. To do this, we consider a generalization of the model studied thus far. In addition to bonding in-

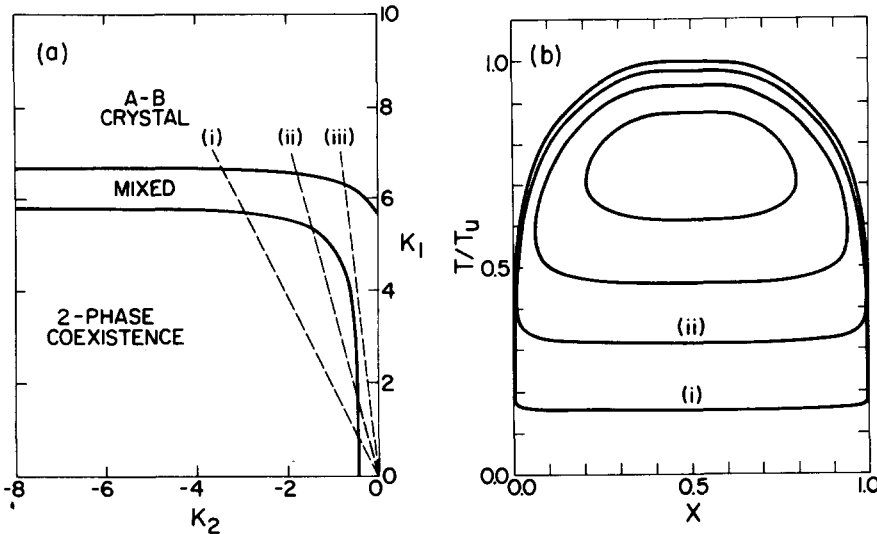


FIG. 4. Results of the trace-out method (Sec. II A) applied to the two-parameter model [Eq. (2)] with $q=500$. (a) Global phase diagram in the relevant quadrant ($K_1 > 0, K_2 < 0$) for binary mixtures showing closed-loop phase diagrams. The boundary separating the "2-phase coexistence" and "mixed" regions is a line of Ising ferromagnetic transitions, while the boundary of the mixed and crystal regions indicates Ising antiferromagnetic transitions. Rays (i) and (ii) represent loci of initial conditions which produce closed-loop $T-x$ phase diagrams. Line (iii) describes a nonseparating system. Note the similarity of the phase diagram to that obtained from the PSRG calculation (Fig. 2). (b) Temperature-composition ($T-x$) phase diagrams for fixed q , showing the evolution of the loops as R increases. Curves (i) and (ii) correspond to the rays (i) and (ii) in (a). All temperatures are normalized to the UCST of (i). Note the flatness of the bottom of the loops, in agreement with many experiments.

teractions between unlike molecules, we include the possibility of bonding between like molecules. The addition of one further interaction to our model generates a three interaction-parameter model^{6,7} (the "generalized model"),

$$-\beta\mathcal{H}_3(K_1, K_2, K_3) = -\beta\mathcal{H}_2 + \sum_{\langle ij \rangle} K_3 \delta_{s_i s_j} \delta_{\sigma_i \sigma_j} \quad (5)$$

A nearest-neighbor pair has reduced energy K_3 if the molecules are of the same type ($s_i = s_j$) and are bonded ($\sigma_i = \sigma_j$). Therefore, the zero energy level is now split into energy K_3 for bonding configurations, and zero for nonbonding configurations, as shown in Fig. 1(b). Notice that again the bonding levels are entropically disfavored relative to nonbonding. We expect many systems to be described by strong bonding between like molecules: Aqueous systems will certainly fall in this class, though at this level we consider the A-A and B-B energies to be the same. Cases in which different types of molecules bond with different strength will clearly be important, and we shall return to this point in Sec. III. For the moment, we can consider K_3 to be roughly the average of the A-A and B-B bonding energies.

It is easy to generate an effective Ising coupling for this model. Consider taking a single bond out of the lattice. This "graph" can be shown to be the leading term in an exact high-temperature series expansion.⁸ The single-bond Hamiltonian is

$$-\beta\mathcal{H}_3(\{s_1, s_2\}; \{\sigma_1, \sigma_2\}) = K_1(1 - \delta_{s_1 s_2}) \delta_{\sigma_1 \sigma_2} + K_2(1 - \delta_{s_1 s_2})(1 - \delta_{\sigma_1 \sigma_2}) + K_3 \delta_{s_1 s_2} \delta_{\sigma_1 \sigma_2} \quad (6)$$

where the subscripts 1 and 2 label the two sites associated with the bond. We now want to trace-out the σ variables to generate an effective Ising coupling. This can be written as

$$\text{Tr}_{\{\sigma_1, \sigma_2\}} \exp[-\beta\mathcal{H}_3(\{s_1, s_2\}; \{\sigma_1, \sigma_2\})] = \exp[-\beta\mathcal{H}_{\text{eff}}(\{s_1, s_2\})] \quad (7)$$

with

$$-\beta\mathcal{H}_{\text{eff}}(\{s_1, s_2\}) = K_{\text{eff}}(1 - \delta_{s_1 s_2}) + K_0 \quad (8)$$

where K_0 is a zero-spin coupling, that is, it simply contributes to the free energy. We can easily carry out this calculation by considering specific configurations for s_1 and s_2 . For example, when $s_1 = s_2 = A$, we obtain

$$\text{Tr}_{\{\sigma_1, \sigma_2\}} \exp(K_3 \delta_{\sigma_1 \sigma_2}) = e^{K_0} = q e^{K_3} + q(q-1) \quad (9)$$

Similarly, when $s_1 = A$ and $s_2 = B$ the result is

$$\text{Tr}_{\{\sigma_1, \sigma_2\}} \exp[K_1 \delta_{\sigma_1 \sigma_2} + K_2(1 - \delta_{\sigma_1 \sigma_2})] = \exp(K_{\text{eff}} + K_0) = q e^{K_1} + q(q-1) e^{K_2} \quad (10)$$

Thus, we readily solve Eqs. (9) and (10) to obtain

$$K_0 = \ln[q e^{K_3} + q(q-1)] \quad (11)$$

$$K_{\text{eff}} = \ln \left[\frac{e^{K_1} + (q-1) e^{K_2}}{e^{K_3} + (q-1)} \right] \quad (12)$$

Using $T = -1/K_2$, and $S = -K_3/K_2$, this can be written as

$$K_{\text{eff}} = \frac{-1}{T} + \ln \left[\frac{\exp[(R+1)/T] + (q-1)}{e^{S/T} + (q-1)} \right] \quad (13)$$

For $S=0$ ($K_3=0$) this reduces to the result given in Eq. (3). Finally, it is clear that this simple trace-out method can be applied to a wide variety of bonding interactions, with equal ease, a definite advantage over the RG calculation. Specifically, the discrete sum over the Potts variables can become an integral over continuous degrees of freedom. Further examples are given in the next section.

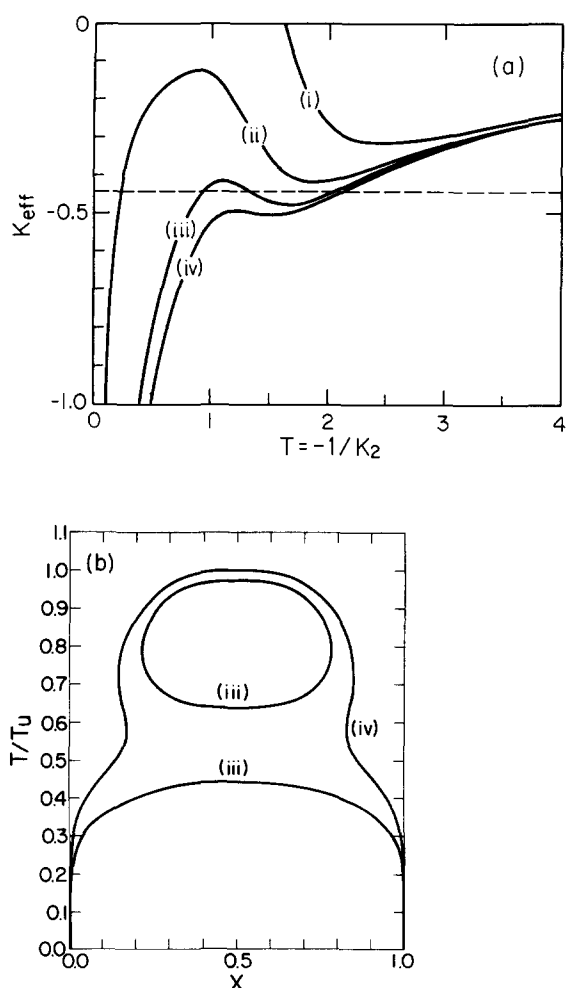


FIG. 5. Results of the trace-out method applied to the generalized Hamiltonian [Eq. (5)]. (a) Nearest-neighbor coupling [for an Ising model written as in Eq. (1)] vs temperature for various values of R at fixed q (500) and S (9.0). Curves (i) through (iv) correspond to $R=9, 8.9, 8.6,$ and $8.5,$ respectively. (b) T - x phase diagrams for curves (iii) and (iv), normalized to the UCST of (iv). Note the "pinched-in" coexistence curve for (iv).

With the expression given in Eq. (13) in hand, we can now explore the phase diagrams which result from this model. First, in Fig. 5(a), K_{eff} is plotted as a function of temperature, for various values of R . For all curves in this figure, q and S are held fixed. We can see that the effective coupling has developed a more complicated temperature dependence with the addition of the interaction K_3 . For example, the system now displays different ground states depending on the relationship of R to S . If $R > S$ ($K_1 > K_3$), then the ground state is as before; namely, A-B [case (i) in Fig. 5(a)]. However, when $S > R$ ($K_3 > K_1$) the ground state is a phase separated system; A-A coexisting with B-B [cases (ii, iii, iv)].

The phase diagrams in T - x space are also considerably more interesting, as shown in Fig. 5(b). Case (iv) ($R < S$) corresponds to (iv) in Fig. 5(a), and we see that there is only a single critical point. Nonetheless, we notice that K_{eff} does not increase in strength monotonically,

but rather, at some low temperature becomes less negative, approaching the critical value, with the result that the phase separation is less complete there. This is reflected in Fig. 5(b) by the "pinching-in" effect exhibited at intermediate temperatures. As R increases K_{eff} evolves to the form in case (iii), where there are now three critical points. The resulting phase diagram in T - x space is shown by (iii) in Fig. 5(b). Inside the loop is the usual two phase coexistence, which reappears at the lowest temperatures. As R is increased further, the loop vanishes, as in Fig. 5(a) case (ii). Finally, when $R > S$, the ground state switches over to A-B. In this particular evolution, the loop vanishes first, as R is increased, and then the lower separation vanishes. For different values of S , the two regions can disappear in reverse order. Thus, we see that an "ordinary" phase separation can pinch in, form a loop, and evolve in various ways as a function of the basic parameters in the model. In the next section we discuss examples of experiments showing these types of phenomena.

Finally, Fig. 6 shows the (K_1, K_2) plane of the global phase diagram for the three interaction-parameter model. We show only the transitions from mixed to two phase coexistence. All curves are calculated with $q = 500$, while S is fixed at various values for the different curves shown. Thus, $S = 0$ is the same phase diagram shown in Fig. 4(a). For a given value of S , the phase boundary asymptotes to a straight line of slope $-S$ as $K_2 \rightarrow -\infty$. This reflects the changeover in the ground state from A-B ($R > S$) to A-A, B-B ($R < S$).

B. Thermodynamic functions

So far, we have studied the model Hamiltonians shown in Fig. 1 both by PSRG methods and a very simple trace-

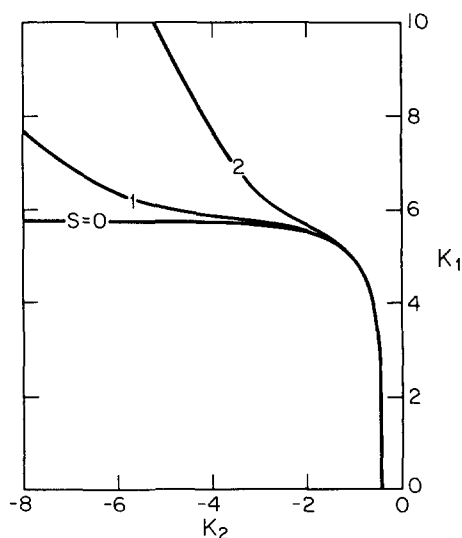


FIG. 6. Global diagram for the Hamiltonian of Eq. (5) for $q = 500$ and various values of S , as indicated. Only the two-phase coexistence boundary is shown. Note the similarity of the three curves near the knee of the ordered region phase boundary. In each case, that boundary asymptotes to a slope of $-S$ as $K_2 \rightarrow -\infty$, $K_1 \rightarrow +\infty$, reflecting the changeover of ground states at $R = S$ ($K_1 = K_3$).

out technique, and presented the various types of phase diagrams that one can obtain. We now turn to a discussion of the basic thermodynamic functions, such as entropy, specific heat, etc., using the trace-out method. We shall see that it is easy to derive analytic expressions for thermodynamic quantities in terms of the Ising model. By then utilizing the information available for the Ising model,^{3,31-33} we are able to study our models in great detail. The results discussed below are in very good agreement with those of the PSRG calculation.

First, we derive an expression for the free energy associated with the general model $-\beta\mathcal{H}_3$ in terms of the Ising free energy. Recall that the results of our trace-out method are contained in Eqs. (11) and (12). To this point, we have basically studied just the implications of Eq. (12), but now, to develop the free energy, we must also include the constant term K_0 as given in Eq. (11). We can see this as follows; the reduced free energy per site ($f = -\beta F$) we desire is

$$f(K_1, K_2, K_3) = \frac{1}{N} \ln \text{Tr}_{\{s_i\}} \text{Tr}_{\{\sigma_i\}} \exp[-\beta\mathcal{H}_3(\{s_i\}, \{\sigma_i\})]. \quad (14)$$

The first step is to carry out the trace over $\{\sigma_i\}$ in an approximate way, as described above, by performing the trace on a single bond. The result is

$$f(K_1, K_2, K_3) \approx \frac{1}{N} \ln \text{Tr}_{\{s_i\}} \exp \left\{ \sum_{\langle ij \rangle} \left[K_{\text{eff}}(1 - \delta_{s_i s_j}) + \frac{1}{2d} K_0 \right] \right\}, \quad (15)$$

where K_0 and K_{eff} are as given before. The factor $1/2d$ in the K_0 term is to prevent over counting the contribution of each site. Recall that each site is a member of $2d$ bonds, where d is the dimensionality of the hypercubic lattice, and each of these bonds contributes a factor of K_0 . We can pull this constant term through the trace, using the relation $\sum_{\langle ij \rangle} 1 = dN$, to obtain

$$f(K_1, K_2, K_3) = \frac{1}{2} K_0 + \frac{1}{N} \ln \text{Tr}_{\{s_i\}} \exp \left[\sum_{\langle ij \rangle} K_{\text{eff}}(1 - \delta_{s_i s_j}) \right], \quad (16)$$

within our approximation. Finally, we wish to make contact with the standard form of the Ising model, which is written

$$-\beta\mathcal{H}_I = \sum_{\langle ij \rangle} K_I s_i s_j \quad (17)$$

where $s_i = \pm 1$. We can express our model in this form by noting that $1 - \delta_{s_i s_j} = \frac{1}{2}(1 - s_i s_j)$. Thus,

$$\begin{aligned} f(K_1, K_2, K_3) &= \frac{1}{2} K_0 \\ &+ \frac{1}{N} \ln \left\{ \exp(N d K_{\text{eff}}/2) \text{Tr}_{\{s_i\}} \exp \left[\sum_{\langle ij \rangle} \left(-\frac{1}{2} K_{\text{eff}} \right) s_i s_j \right] \right\} \\ &= \frac{1}{2} K_0 - d K_I + f_I(K_I), \end{aligned} \quad (18)$$

with

$$K_I = -\frac{1}{2} K_{\text{eff}}. \quad (19)$$

Note that the effective Ising coupling is now > 0 for ferromagnetic ordering, since we have mapped onto the Hamiltonian in Eq. (17). This is the basic result relating the thermodynamics of the model we study to the Ising model. In future usage, the subscript I will always refer to the standard Ising model as written in Eq.

(17), while quantities with no subscripts refer to the model $-\beta\mathcal{H}_3(K_1, K_2, K_3)$.

One of the simplest thermodynamic quantities to consider is the spontaneous magnetization. Since K_0 and $K_I = -\frac{1}{2} K_{\text{eff}}$ are both analytic functions, they will not contribute, and thus we simply have

$$\Delta M(K_1, K_2, K_3) = \frac{1}{2} \lim \left[\left(\frac{\partial f}{\partial h} \right) \Big|_{h=0^+} - \left(\frac{\partial f}{\partial h} \right) \Big|_{h=0^-} \right] = \Delta M_I(K_I), \quad (20)$$

where h is the magnetic field. For the purposes of a T - x phase diagram recall that we make the association $x_{\pm} = \frac{1}{2}(1 \pm M)$.

Next, consider the entropy. In terms of the reduced free energy, the entropy is

$$s = f + T(\partial f / \partial T). \quad (21)$$

Recall that we define temperature to be $T = -1/K_2$, from which it follows that $\partial K_1 / \partial T = -RK_2^2$, $\partial K_2 / \partial T = K_2^2$, and $\partial K_3 / \partial T = -SK_2^2$. Using these relations, we find,

$$\begin{aligned} s &= f + T \left[\left(\frac{\partial f}{\partial K_1} \right) \left(\frac{\partial K_1}{\partial T} \right) + \left(\frac{\partial f}{\partial K_2} \right) \left(\frac{\partial K_2}{\partial T} \right) + \left(\frac{\partial f}{\partial K_3} \right) \left(\frac{\partial K_3}{\partial T} \right) \right] \\ s &= f - \left[K_1 \left(\frac{\partial f}{\partial K_1} \right) + K_2 \left(\frac{\partial f}{\partial K_2} \right) + K_3 \left(\frac{\partial f}{\partial K_3} \right) \right]. \end{aligned} \quad (22)$$

In terms of the Ising model, this is

$$\begin{aligned} s &= f_I - d K_I + \frac{1}{2} K_0 - \frac{1}{2} K_3 \left(\frac{\partial K_0}{\partial K_3} \right) \\ &+ \left(d - \frac{\partial f_I}{\partial K_I} \right) \left[K_1 \left(\frac{\partial K_I}{\partial K_1} \right) + K_2 \left(\frac{\partial K_I}{\partial K_2} \right) + K_3 \left(\frac{\partial K_I}{\partial K_3} \right) \right]. \end{aligned} \quad (23)$$

This is to be compared with the Ising entropy which is

$$s_I = f_I - K_I \left(\frac{\partial f_I}{\partial K_I} \right). \quad (24)$$

With these results we can study some of the aspects of this model which were simply mentioned in a qualitative manner above. In particular, it is clear that below the closed loop the entropy of mixing has increased, though, of course, we expect that the total entropy decreases monotonically as temperature is lowered. This can happen if the decrease in orientational entropy is more than enough to offset the increase in mixing entropy. To study this quantitatively, we first note that Eq. (23) is an expression for the total entropy of the system, i.e., orientational plus mixing. On the other hand, the mixing entropy is simply the entropy associated with the Ising degrees of freedom, which is given in Eq. (24). Clearly, the orientational entropy is just the difference. In Fig. 7 we plot the various entropies for the case of a typical loop. Note that the temperature axis is now horizontal, and that one vertical axis is associated with composition, the other with the entropies. First, in Fig. 7 curve (a), we plot the mixing entropy, which, near the bottom of the loop, increases as the system becomes homogeneous. The decrease in orientational entropy (b) is enough so that the total entropy, curve (c), does decrease monotonically with T . Thus, the basic mechanism of the model is explicitly illustrated in this calculation.

Let us now consider the specific heat (at $h=0$) defined

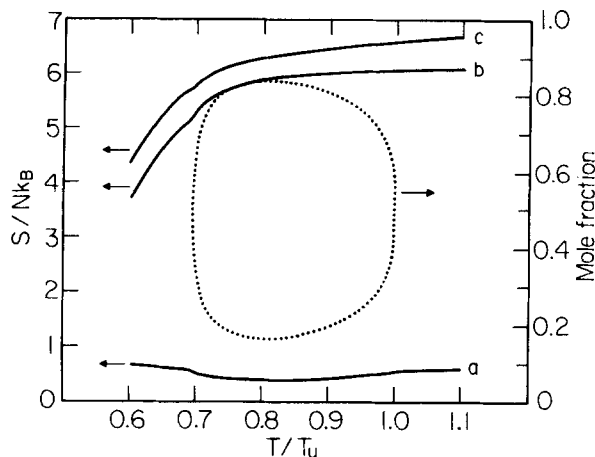


FIG. 7. Mixing, orientational, and total entropy [(a), (b), and (c), respectively] for a typical closed-loop phase diagram. Note the normalization of the temperature scale to the UCST of the loop. The mixing entropy increases as the loop closes up, near the LCST, as expected, while the orientational entropy decreases rapidly enough, as the system settles into A-B bonded states, that the total entropy monotonically decreases.

by the relation

$$C = T \left(\frac{\partial s}{\partial T} \right), \quad (25)$$

where s is given in Eq. (23). It should be pointed out that, since our model is symmetric, this is simply the specific heat at constant composition $x = \frac{1}{2}$. After some straightforward, but tedious algebra, we obtain

$$C = \left[\left(\frac{\partial f_I}{\partial K_I} \right) - d \right] \left[K_1^2 \left(\frac{\partial^2 K_I}{\partial K_1^2} \right) + K_2^2 \left(\frac{\partial^2 K_I}{\partial K_2^2} \right) + K_3^2 \left(\frac{\partial^2 K_I}{\partial K_3^2} \right) \right. \\ \left. + 2K_1 K_2 \left(\frac{\partial^2 K_I}{\partial K_1 \partial K_2} \right) + 2K_2 K_3 \left(\frac{\partial^2 K_I}{\partial K_2 \partial K_3} \right) + 2K_1 K_3 \left(\frac{\partial^2 K_I}{\partial K_1 \partial K_3} \right) \right] \\ + \left(\frac{\partial^2 f_I}{\partial K_I^2} \right) \left[K_1 \left(\frac{\partial K_I}{\partial K_1} \right) + K_2 \left(\frac{\partial K_I}{\partial K_2} \right) + K_3 \left(\frac{\partial K_I}{\partial K_3} \right) \right]^2 + \frac{1}{2} K_3^2 \left(\frac{\partial^2 K_0}{\partial K_3^2} \right). \quad (26)$$

By comparison, the Ising specific heat is simply

$$C_I = K_I^2 \left(\frac{\partial^2 f_I}{\partial K_I^2} \right). \quad (27)$$

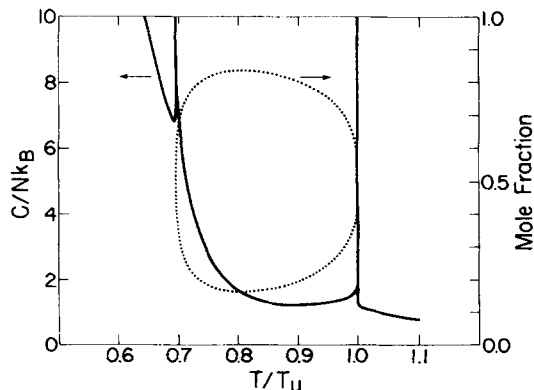


FIG. 8. Specific heat calculated from Eq. (26) for a typical closed-loop phase diagram obtained from the two-parameter model [Eq. (2)]. Note the reversal of the amplitudes at the LCST. The dramatic rise of the background at low temperatures signals the approach of the transition to the A-B crystal.

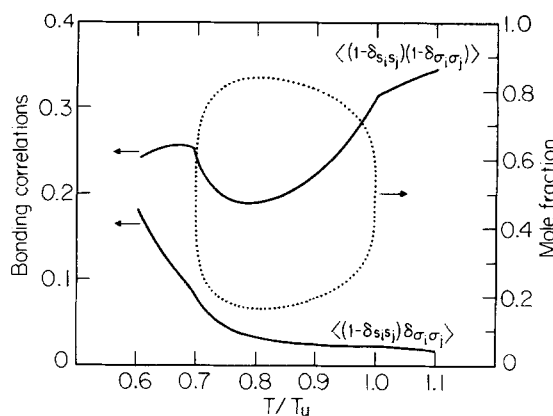


FIG. 9. Nearest-neighbor bonding correlations vs temperature for a closed-loop phase diagram. The lower curve shows the fraction of "bonded" unlike nearest neighbors [Eq. (28)], and the upper curve gives the fraction of nonbonded unlike nearest neighbors [Eq. (29)]. Note that bonding does not become significant until near the LCST.

Figure 8 shows the specific heat for a typical closed-loop diagram. Note how the amplitudes of the specific heat are reversed for the lower critical point as compared to the upper, in agreement with experiments.¹⁹ The large background at temperatures below the LCST signals the approach of the transition to the "crystal" phase.

It is also of interest to study various nearest-neighbor correlations of the model. For instance, the fraction of nearest neighbors which are unlike and orientationally bonded (A-B) is

$$\langle (1 - \delta_{s_i s_j}) \delta_{\sigma_i \sigma_j} \rangle = \frac{1}{d} \left(\frac{\partial f}{\partial K_1} \right) = \left[\frac{1}{d} \left(\frac{\partial f_I}{\partial K_I} \right) - 1 \right] \left(\frac{\partial K_I}{\partial K_1} \right). \quad (28)$$

This function is shown in Fig. 9, where we can see that the fraction of bonding increases dramatically in the vicinity of the LCST, in accord with the mechanism described in the Introduction. Similarly, we can determine the fraction of nearest neighbors which are unlike and not bonded (A·B) to be

$$\langle (1 - \delta_{s_i s_j})(1 - \delta_{\sigma_i \sigma_j}) \rangle = \frac{1}{d} \left(\frac{\partial f}{\partial K_2} \right) = \left[\frac{1}{d} \left(\frac{\partial f_I}{\partial K_I} \right) - 1 \right] \left(\frac{\partial K_I}{\partial K_2} \right), \quad (29)$$

which is also plotted in Fig. 9. The large drop in this quantity within the loop is due to the fact that when the system phase separates, most nearest neighbors are AA and BB.

Finally, we consider the nearest-neighbor correlation of the Ising variables $\langle s_i s_j \rangle$. Since the Ising variables relate to the composition of the fluid, it is such correlations which contribute strongly to scattering, e.g., in a light scattering experiment. The solid curve in Fig. 10 is $\langle s_i s_j \rangle$ associated with the closed-loop coexistence curve. The dashed curve shows the same correlation, but for a system in which the loop has just vanished, i.e., R has just become large enough that phase separation no longer occurs. Though the system is now miscible at all temperatures, we see that the correlation still has a maximum just where the system is closest to phase separating. Thus, in a totally miscible sys-

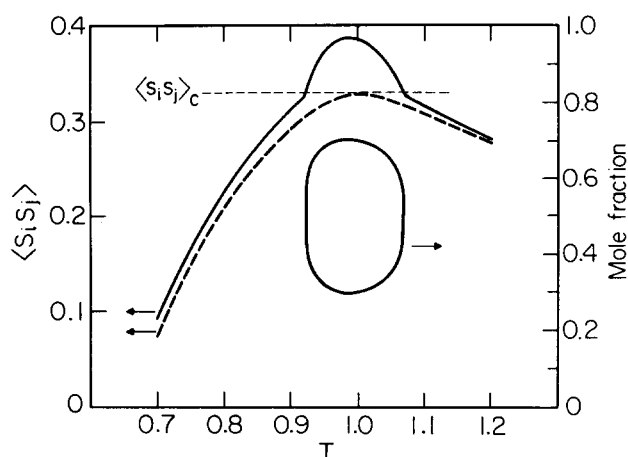


FIG. 10. Nearest-neighbor correlation function $\langle s_i s_j \rangle$ for $q = 500$ and R greater (less) than the critical R for the loops to form (dashed and solid curves, respectively). The critical coupling $\langle s_i s_j \rangle_c$ for phase separation to occur is indicated. Note the distinct maximum present even when no miscibility gap appears (dashed curve).

tem, the correlation $\langle s_i s_j \rangle$ gives a clear indication of an incipient closed loop. If an experimental variable, such as pressure or the composition of a third component, is changed in the appropriate direction, the maximum of $\langle s_i s_j \rangle$ will rise until it reaches the critical value $\langle s_i s_j \rangle_c$, beyond which the loop appears. Therefore, the study of correlations, in particular those measured by light scattering, can identify systems which may look simple, but in fact are likely to show closed-loop behavior. Of course, scattering experiments measure quantities which are not simply nm correlations, but we expect a rise in $\langle s_i s_j \rangle$ to be indicative of the onset of long-range correlations. A further discussion of this is given in Sec. III D.

III. THEORETICAL PREDICTIONS, INTERPRETATION OF MODELS, AND COMPARISONS WITH EXPERIMENTS

In the following section, we discuss the use of the WV models in the interpretation of experimental data on binary systems. While the models' parameters are typically well defined in matching experiments, the interpretation of their trends is not always straightforward. However, our goal in this work is not the formulation of a detailed microscopic theory of these parameters, with specific systems in mind. Rather, in this paper we study simple methods of fitting the parameters to a wide range of experimental data and extracting the dominant trends. In cases where the underlying physics is clear, we will expand upon the discussion.

A. Isotope substitution experiments

One of the most straightforward experiments on binary mixture miscibility is the study of the effects of progressive enrichment of one component with one of its isotopic variants. Cox¹⁵ has studied the dependence of critical solution temperatures in the 3-methyl pyridine + D₂O system on progressive dilution of the D₂O with H₂O, while keeping the total pyridine weight fraction

in the mixture constant. The results are indicated by the stars in Fig. 11. Our method for fitting the two-parameter model [Eq. (2)] to this data is straightforward: For a reference system we use the pure D₂O T - x data. The parameters q and R are chosen to reproduce exactly the ratio LCST/UCST, and give good agreement with the observed width of the coexistence curve. We have used the symmetrization procedure described by Johnston *et al.*,³⁶ to allow comparison between the data and the symmetric lattice-gas phase diagrams. The precise value of q for optimum match to this reference curve width is not important, since we are interested in trends in the parameters with a perturbation such as isotopic dilution. The value of q (500) for pure D₂O was also chosen based on consideration of the approximation acceptance angle of a hydrogen bond. We have found that values of q of ~ 500 are applicable to a wide range of systems. For each pair of data points at a given mole fraction of H₂O in the solvent, the values of q and R relative to the pure D₂O system are uniquely defined: Both the miscibility gap critical point temperature ratio and the ratios of those points to the pure D₂O points must be satisfied. Matching the gap ratio alone is not sufficient for a unique determination of q and R and will not, in general, produce an internally consistent experimental match. The trends in these parameters are shown in Fig. 12. They show a remarkably linear dependence on solvent composition, suggesting that the effective interactions are just composition averages of the intrinsic H₂O and D₂O properties. In Fig. 11 we show the agreement with the experiments obtained by a simple linear interpolation between the values of R and q at the extremes of composition. We predict that the loops vanish at a mole fraction $x_{\text{H}_2\text{O}} = 0.815$, in the solvent, in a solution of 30% β -picoline by weight.

The actual strength of the bonding interaction can be calculated as follows: The temperature scale we use

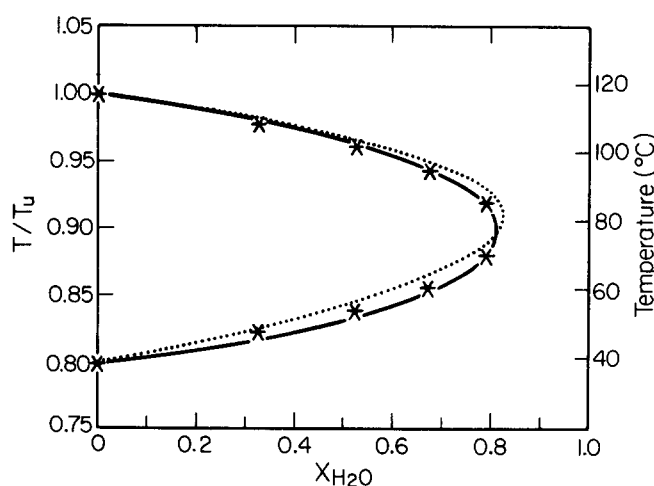


FIG. 11. Miscibility gap critical temperatures for the system 3-methyl pyridine + H₂O + D₂O, as a function of the isotopic composition of the solvent. Data are from Ref. 15 and normalized to the pure D₂O UCST. The heavy line is the result of a calculation in which q and R are linearly interpolated between the values chosen to fit the data at the extremes of composition. The dotted line is the fit using Eqs. (30)–(32), holding q at 500.

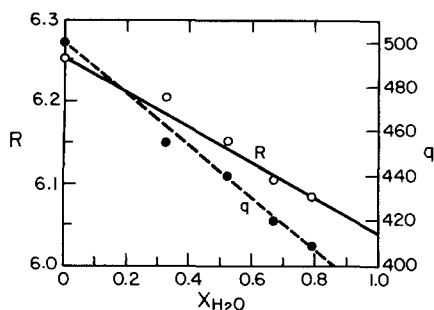


FIG. 12. Trends in the parameters R and q with the solvent composition of the mixtures for the system 3-methyl pyridine + $\text{H}_2\text{O} + \text{D}_2\text{O}$. The lines between the data at the extremes of composition show the linear interpolations which are used in Fig. 11.

is $K_2 = -1/T$, and thus the point-by-point match to the data fixes J_2 to be $-k_B T_u K_2$, where T_u is the UCST for $x_{\text{H}_2\text{O}} = 0$. For the β -picoline system this is +0.41 kcal/mol. The bonding interaction is just $-R J_2$ and this is displayed as a function of the solvent composition in Table I. The calculated values are reasonable estimates of hydrogen bond strengths (relative to the non-bonding interaction J_2) and decrease in strength with added H_2O , as discussed below. This type of analysis can also be done by fixing q and letting K_1 and K_2 vary freely. It is again found that J_2 is approximately constant, while J_1 becomes less negative with added normal water, as above.

While our model is by no means a detailed microscopic theory of the complexities of hydrogen bonding, the above results are suggestive of a simple explanation for the observed behavior. Based on the Born-Oppenheimer approximations to a chemical bond, one would expect the intermolecular potential wells for a hydrogen bond and a deuterium bond to be essentially identical. The deuteron would lie lower in the well than the lighter proton, and hence be held more strongly. Thus, the system average strength of the unlike molecule attractive force R should decrease with progressive addition of normal water. Note that a hydrogen atom has a larger thermal de Broglie wavelength than a deuterium atom and hence is less localized (and therefore has a lower q). Within our model, a decreasing unlike attractive energy R for constant q , is accompanied by an increasing miscibility gap. Thus, in order for the loop to shrink, there must be a simultaneous decrease in the orientational specificity. This is equivalent to q decreasing. In the global phase diagram [Fig. 4(a)], the height of the two phase coexistence boundary scales as $\ln q$ and therefore a decrease in q will tend to move the boundary down, decreasing the size of the miscibility gap. Thus, these arguments allow for a consistent interpretation of the results shown in Fig. 12, but do not, of course, rule out the possibility of other explanations.

Although the parameter fitting in the 3-methyl pyridine + $\text{H}_2\text{O} + \text{D}_2\text{O}$ system is clearly defined, there may be other systems for which a simple approximation is useful for a qualitative description of miscibility trends. If the perturbation to the system is small, it may be

reasonable to assume that either one of q or R is roughly constant throughout the perturbation. For instance, in the $\text{H}_2\text{O}/\text{D}_2\text{O}$ case above, instead of following the correct procedure of generalizing the Hamiltonian explicitly to account for a third interacting species, with an associated chemical potential, we can gain a rough idea of the results by simply performing the trace over the Potts variable (see Sec. II A) assuming a fraction $(1-p)$ of the unlike nearest-neighbor pairs interacts with one bond strength R , and a fraction p interacts with strength R' . We then interpret p as, for instance, the mole fraction of H_2O in the solvent. This procedure leads to a very simple result, but we emphasize again that this is not a correct statistical mechanical approach to the problem, and that certain difficulties in interpretation could arise.

The effective coupling in this approximation then becomes

$$K_{\text{eff}} = \frac{-1}{T} + \ln \left\{ 1 + \frac{1}{q} \left[(1-p) e^{(R+1)/T} + p e^{(R'+1)/T} - 1 \right] \right\}. \quad (30)$$

Recall that the system maps onto the standard Ising model via $K_I = -(\frac{1}{2})K_{\text{eff}}$. The parameter R' can be determined uniquely from the data by noting that we can define an effective R , through the relation

$$e^{(R_{\text{eff}}+1)/T} = (1-p) e^{(R+1)/T} + p e^{(R'+1)/T}. \quad (31)$$

We then require that R_{eff} be the critical value of R such that the locus of initial conditions is tangent to the Ising critical surface (as in Fig. 13) for that value of p at which the miscibility gap vanishes. Denoting that temperature T_c (in reduced units), and critical p by p_c , we find

$$R' = R_c \ln \left\{ \frac{e^{R_c/T_c} - (1-p_c) e^{R/T_c}}{p_c} \right\}, \quad (32)$$

where R is fixed by matching the data at $p=0$. The results of such a match to the pyridine-water data are moderately good (see Fig. 11). We find that the agreement is fairly insensitive to small changes in q , but does improve for very much lower q (~ 50) and appropriate values of R . Similar results can be obtained by assuming both species have the same strength of interaction but different orientational specificities q and q' .

TABLE I. Calculated hydrogen bond strengths as a function of the composition of the solvent $\text{H}_2\text{O} + \text{D}_2\text{O}$ for the system 3-methyl pyridine + $\text{H}_2\text{O} + \text{D}_2\text{O}$. For this calculation, the nonbonding energy is constant at $J_2 = +0.41$ kcal/mole. Values of q and R for this calculation are shown in Fig. 12. Note that the bonding interaction becomes less favorable as the solvent is made richer in normal water (see text for discussion).

Mole fraction H_2O in $\text{H}_2\text{O} + \text{D}_2\text{O}$	J_1 (kcal/mole)
0.000	-2.58
0.523	-2.54
0.790	-2.51

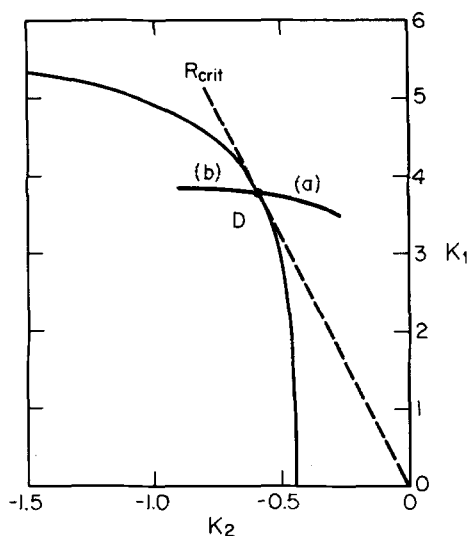


FIG. 13. Detail of the global phase diagram in Fig. 4(a), showing a locus of initial conditions (dashed line) such that the miscibility gap has just vanished. Curve (a) shows, in this parameter space, the points of maximum nn correlation, as R varies for fixed q . The continuation of (a) into the phase separated region, illustrated by Sec. (b), is the locus of maximum phase separation as R is varied further. Thus, Sec. (a) represents the locus of closest approach to criticality while (b) represents the greatest distance from the critical surface, within the loop. Critical exponents are predicted to be re-normalized at the point D.

The determination of which approximation is more physically reasonable depends of course on the specific molecular system being studied.

B. Studies of the pressure dependence of miscibility

Much experimental work has been performed on the pressure dependence of miscibility gaps in organic mixtures. While, as noted in the Introduction, a T - p - x miscibility dome is a common occurrence, there are other phenomena for which a mechanistic understanding and physical models are useful. In this subsection, we explore several of these with the two lattice-gas Hamiltonians to show that they contain the essential physics manifested in complicated experimental data. Agreement with data is achieved with a minimum of parametric freedom.

The binary system 2-butanol + H_2O has been studied for many years^{37,38} (starting in the very early part of this century). At high pressures, a simple T - p - x miscibility dome is observed with the "hypercritical point" (at which the gap disappears) located at ~ 845 atm and $\sim 67^\circ C$.³⁷ At pressures below ~ 200 atm, the T - x diagram at a fixed pressure ceases to show a closed loop. Instead, the system remains separated from the UCST all the way to a freezing transition. However, the coexistence curve is pinched in at low temperatures, suggesting an evolution of phase diagrams as in Fig. 14(a) and 14(b). Note that the global phase diagram of the general model, in the region of the "knee" of the ferromagnetic boundary, is very similar to that of the $S=0$ model (Fig. 6). We thus can study the 2-butanol

+ H_2O system at high pressures with the two-parameter Hamiltonian to a good approximation. Of course, at lower pressures, the full three-parameter model must be used. An example of a matching of experimental data for a system with a lower separation is discussed below.

Our method of fitting the values of q and R to the pressure data is totally analogous to that used in the $H_2O + D_2O + 3$ -methyl pyridine data: We choose a reference system (in this case, the 200 atm coexistence curve) and for each pressure adjust q and R to give the correct miscibility gap ratio and LCST and UCST ratios to the reference critical points. As in many binary aqueous mixtures, the T - x coexistence curves are asymmetric with respect to mole fraction 1/2. Often, as is the case here, considerable symmetrization is achieved with a change of variables from mole fraction to weight fraction, reflecting the very small size but moderate density of water molecules relative to the larger organic species. The symmetrization procedure of Johnson *et al.*³⁶ used before, provides a convenient method of comparison with these lattice-gas predictions. The results of such a fit are shown in Fig. 15, where we compare the WV predictions of the T - x curves with the data over a wide range of pressure (~ 650 atm). Once having fit the values of the LCST and UCST, the theoretical coexistence curves (Fig. 15) are in very good agreement with

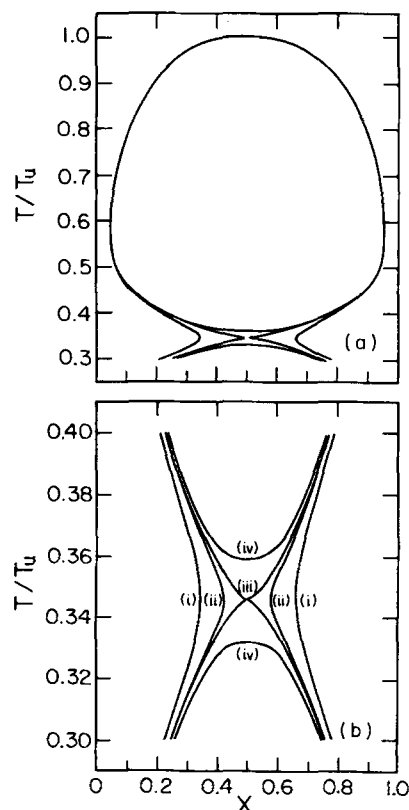


FIG. 14. Evolution of phase diagrams obtained from the generalized Hamiltonian, Eq. (5), for a fixed q (500) and S (6, 5) and slightly varying R . Note in (a) how the curve develops a critical double point and then forms a closed loop with a lower separation. (b) Detail of the lower separation region of (a). $R=6.200$ (i), 6.204 (ii), 6.204418... (iii), and 6.206 (iv).

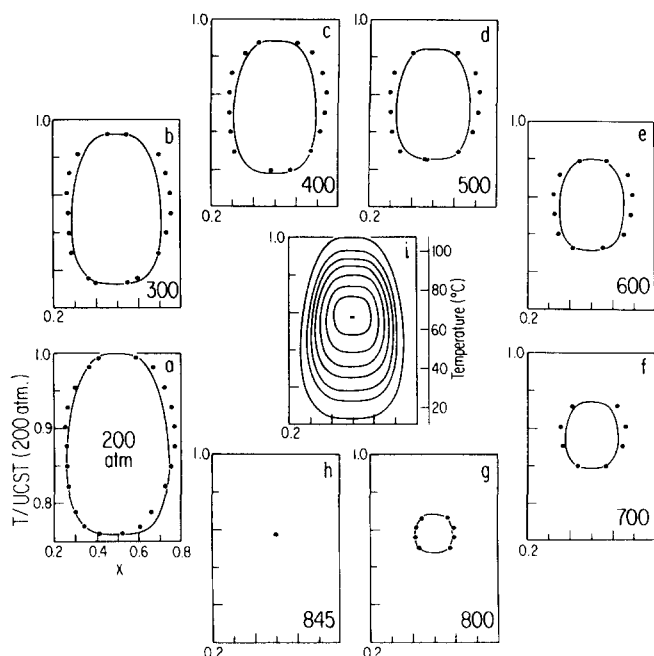


FIG. 15. Comparison of the T - x phase diagrams predicted from the two-parameter model with experiments on 2-butanol + H_2O . Data are from Ref. 37. The values of q and R used for each pressure are those in Fig. 16, determined by requiring the correct LCST/UCST ratio, and critical point ratios relative to the 200 atm data. The shape of the curves is a result of the calculation. The data have been symmetrized by the method of Ref. 36. Curves in (a) through (h) are all normalized to the UCST at 200 atm. (i) Superposition of the theoretical curves in (a) through (h), showing a projection of the T - p - x miscibility dome on the T - x plane.

the experimental data. It is interesting to note the very regular trends in the shapes of the coexistence curves when seen superimposed as in Fig. 15(i). The fact that the theoretical curves for intermediate pressures are systematically slightly narrower than the data is a characteristic of the trace-out method: The full Migdal-Kadanoff calculation would fit better, although be much more involved to implement. Although there appear to be systematic trends in the dependence of q and R on pressure (see Fig. 16), a microscopic interpretation is not yet clear because of complications associated with the compressibility of the real system and the fixed spacing of the lattice-gas model, as well as other factors. However, the magnitudes of the interaction energies in this system are similar to those of the 3-methyl pyridine system discussed above.

Poppe³⁹ has studied the pressure dependence of the miscibility of the binary system glycerol + guaiacol (*o*-methoxy phenol) with small amounts of water (< 2.5% by weight). We note that, while several recent workers^{5, 8, 23, 24} have compared lattice-gas models to this system, no mention has been made of Poppe's observation that anhydrous glycerol and guaiacol are miscible in all proportions and at all temperatures. Only after the introduction of ~ 1.14% water does the system begin to show a small miscibility gap. It is inferred³⁹ that the often quoted study of McEwan⁴⁰ was conducted with a mix-

ture containing ~ 2.88% water. Since glycerol is hygroscopic, it is not unreasonable that water contamination occurs. That this system is so sensitive to the addition of a polar molecule such as water, and considering the Hirschfelder, Stevenson and Eyring⁹ hypothesis (see Sec. IA), we suggest the following interpretation of the trends of phase separation: The water molecules compete for hydrogen-bonding sites on both glycerol and guaiacol, thereby reducing the attractive forces between the unlike molecules. It thus becomes energetically less favorable for the system to remain mixed. We expect that the anhydrous mixture would show precritical behavior, as might be detected in scattering experiments or thermodynamic measurements (see Sec. III D).

Within the context of our two-parameter model, we can attempt to describe the above effects by variation of the coupling-strength ratio R while keeping q fixed. Of course, hydration effects may also change the orientational specificity of the bonding. The effect on the coexistence curves is qualitatively the same. There are two sets of experimental data which we fit with our model. The first is simply the trends in the UCST and LCST with increasing concentration of water, at fixed pressure. The second is variation in critical solution temperatures with pressure, at fixed composition.

The data on the miscibility gap as a function of the weight percent of water, at atmospheric pressure, has been fit by linearly interpolating R between the appropriate value at 2.28% water and the critical value at ~ 1.14%. While there is some uncertainty in the exact position of the vanishing of the closed loops, the fit to the data is fairly insensitive to that exact value, except as the loop shrinks, near 1.20% water (Fig. 17).

It should be noted that the sizes of the closed loops in the glycerol + guaiacol + H_2O mixtures, as measured by the quantity $(1 - LCST/UCST)$, are very small in comparison with other systems studied. Also, the variations in the UCST and LCST near the top of the T - P - x domes are essentially symmetric (see Fig. 17). This is to be contrasted with the variation of the loops in the systems

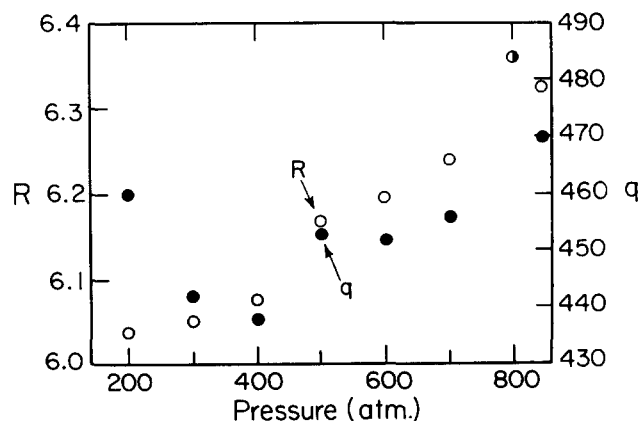


FIG. 16. Results of a point-by-point match of the parameters q and R to the critical solution temperature data on the system 2-butanol + H_2O above 200 atm (Ref. 37). Note the reversal of the trends in q and R relative to those found in the 3-methyl pyridine + H_2O + D_2O system (Fig. 12).

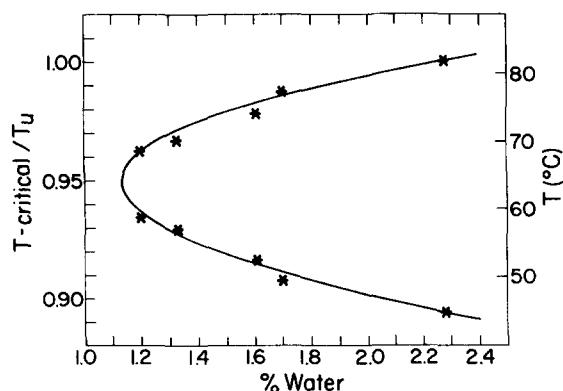


FIG. 17. Critical solution temperatures as a function of weight percent water for the system glycerol + guaiacol + H_2O . The theoretical curve is calculated by a linear interpolation of R from a reference value at 2.28% water to the critical value for the loops to vanish (for $q=500$) at 1.14% water. The normalization temperature is the UCST of the 2.28% water system. Data are from Ref. 39.

2-butanol + water, and 3-methyl pyridine + H_2O + D_2O , discussed above. In our model, as either q or R is varied to bring the minimum in the Ising coupling constant near the Ising critical surface, the gap will be predicted to vanish parabolically, also. Hence, for these small loops a distinction between pressure induced changes in the orientational specificity (q) and the strength of bonding interactions (R) is difficult to make. Below we show the agreement between the choices in this system.

The results of fitting the pressure studies data by linearly interpolating q between a reference value at the lowest pressures studied and the critical q for the loops to vanish is shown in Fig. 18. Note that all three of the curves are fit by assuming the same R and adjusting q

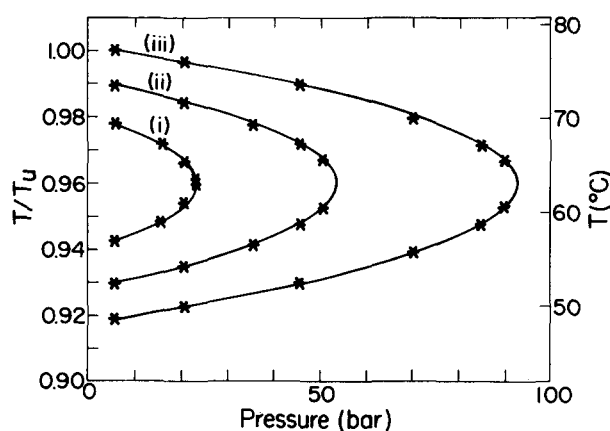


FIG. 18. Pressure dependence of critical solution temperatures for the system *o*-methoxy phenol (guaiacol) + glycerol with varying amounts of water. Data for curves (i), (ii), and (iii), are, respectively, for 1.35%, 1.61%, and 1.90% water by weight. Note that the addition of water decreases the mutual solubility of the two compounds. All temperatures are normalized to the 1.90% water low pressure UCST. Data are from Ref. 39. The theoretical curves are calculated by a linear interpolation of q , for fixed R , from the reference value at low pressure to the pressure at which the closed loops vanish.

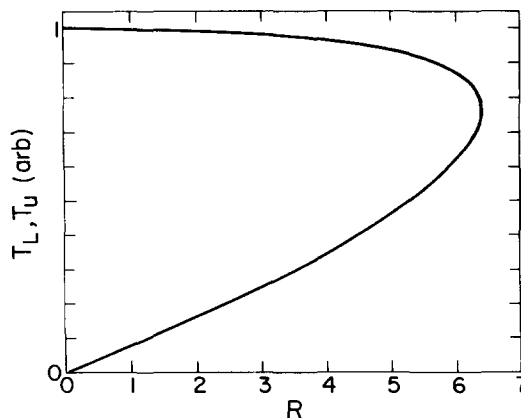


FIG. 19. Theoretical variation in critical solution temperatures with a wide variation in R , for $q=500$. Temperatures are normalized to the UCST for $R=0$. Note the roughly parabolic behavior near the vanishing of the loops ($R \sim 6.4$) and the decided asymmetry as the loops widen (decreasing R).

to match the gap ratio at low pressure and produce the correct hypercritical point. This is essentially a one parameter fit to the data and therefore the match to the two temperature ratio constraints (discussed before) can not be satisfied, in general. However, even with this restricted freedom, the agreement with the data is very good. The agreement between the model parameters obtained in this fit and those of the previous one (extrapolated to a common pressure) is very good.

For systems with larger loops, it is observed that, as a function of concentration of a third component, or pressure, etc., the LCST rises much faster than the UCST falls, as the loop vanishes.^{12,13} Figure 19 shows that the predicted trends, based on holding q at 500 and linearly varying R , are in agreement with the experiments. From the global phase diagram [Fig. 4(a)], this behavior is clear since the point L rapidly recedes to infinity (zero T) as R decreases, while the location of point U varies much more slowly. The decorated lattice models show a much more symmetric, almost parabolic behavior for low directional specificity to the bonding,²³ but agree qualitatively with our calculations for highly directional bonds.⁴¹ Similar results from the WV models come from a variation in q at fixed R .

To emphasize the physical relevance of the three-parameter model, we study the data on the system ethanol + water + K_2CO_3 . Novak and Schneider⁴⁴ have reported the pressure dependence of the miscibility critical points, at various concentrations of the electrolyte K_2CO_3 . Figure 20 shows some typical experimental results. Note that ethanol and water are miscible in the absence of salts. The observed widening of the region of immiscibility (for a fixed pressure) with increasing electrolyte concentration is a result of the well known "salting out" effect^{42,43} As the concentration of ions in solution is increased, the polar hydroxyl groups of both components become increasingly electrostatically shielded from one another, reducing the strength of the hydrogen bond and dipolar attractive forces. Hence, at a given temperature, with added salts, it becomes less favor-

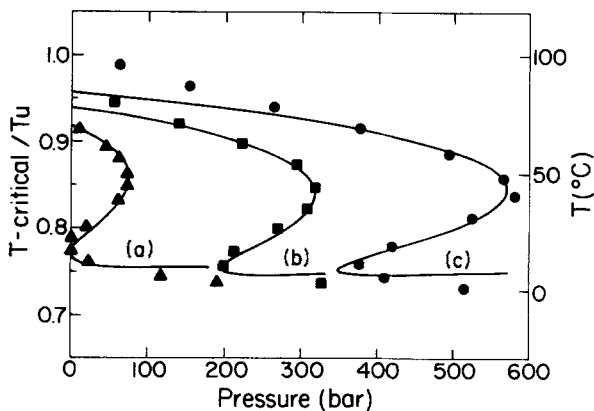


FIG. 20. Critical temperatures as a function of pressure for the system ethanol + H_2O + K_2CO_3 at various concentrations of the electrolyte: (a) 14.00% by weight, (b) 14.40%, and (c) 14.90%. Data are from Ref. 14. Normalization is to the 1 atm extrapolated value of the 14.90% curve. The solid curves are fits to the data, as described in the text, by linear interpolations and extrapolations from the values of R and S at two reference pressures, with q fixed at 500. Typical values of R and S are 9.3 and 10.5 respectively, with their pressure derivatives on the order of $(5-10) \times 10^{-4} \text{ bar}^{-1}$. Hence, the T - x phase diagrams change very rapidly as a function of the model parameters.

able for the system to be mixed than to separate (or phase separate further) with the associated loss of entropy of mixing and gain in orientational entropy. The generalized Hamiltonian in the high-temperature series expansion can predict such behavior by variation of the appropriate energy parameters.

To fit this model to the data, we locate four reference points in the p - T diagram. These are labeled in Fig. 21(a). We choose these points because, within the trace-out method, the behavior of K_{eff} with temperature is very clearly defined, as Fig. 21(b) indicates. At this stage of developing our models, we seek only to demonstrate that a minimum of parametric variation can produce this type of phase diagram, and thus we do not optimize the fit except by eye. In this spirit, we have fixed the parameter q at 500 and adjusted R to put the four reference points in good agreement with the data. This is also a one-parameter fit since S is uniquely determined by q and R , and the constraints on the temperature dependence of K_{eff} . The theoretical curves in Fig. 20 are calculated by linear interpolations and extrapolations of R and S from those two reference pressures. Considering the simplicity of the matching procedure, the results are very encouraging. The expected evolution of T - x phase diagrams for the middle curve in Fig. 20 is shown in Figs. 22(a)–22(c). It appears that this system is analogous to the 2-butanol + water curves, except that in the latter the lower separation was not detected. The data of Moriyoshi *et al.*³⁷ were taken at pressure increments of ~ 100 atm. We suggest that a finer interval would detect such a separation [as in Fig. 14(b)].

C. Exponent renormalization in the trace-out method

The temperature-dependent coupling constant which arises in the trace-out map to the Ising model can cross

the Ising critical surface as many as three times in a temperature scan [for fixed values of q , R , and S , as in Fig. 5(a)]. For the general case of these parameters, these critical points are distinct. Of course, for specific values, as shown above, two or even all three of these critical points can merge, leading to “renormalized” exponents for the various thermodynamic singularities.^{7,25,44} These can be examined in scattering experiments, order parameter measurements or specific heat studies. For mathematical convenience, we discuss in detail only the case of the merging of the two critical points in the basic two-parameter model. More complex phenomena in the generalized model can be

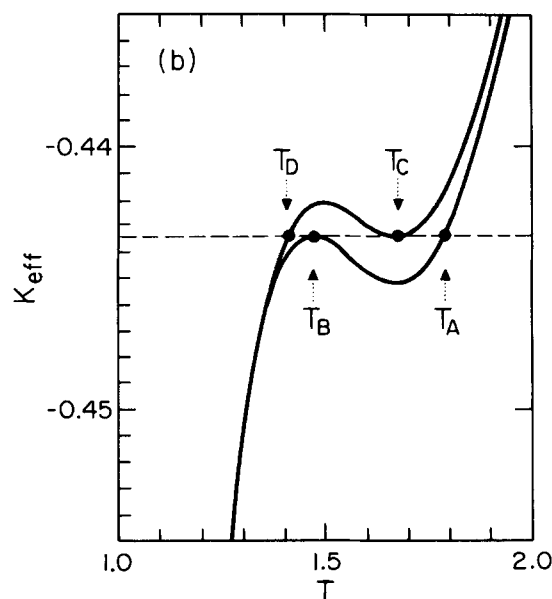
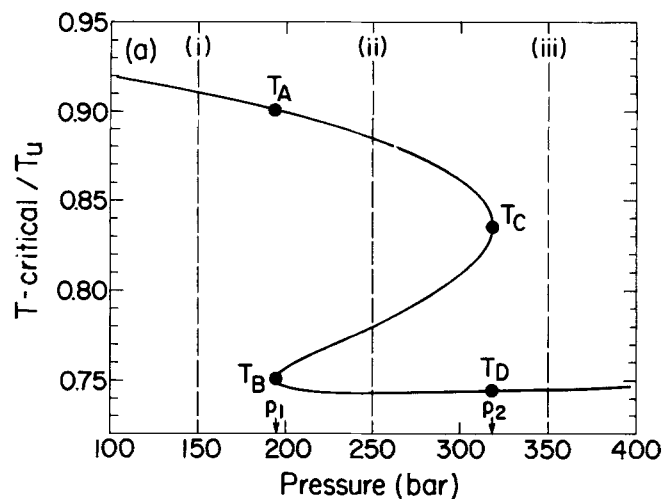


FIG. 21. Method of fitting the generalized Hamiltonian parameters to complex miscibility data. (a) Detail of curve (b) of Fig. 20, showing idealized reference points T_A , T_B , T_C , and T_D at two reference pressures p_1 and p_2 . The fitting procedure described in the text attempts to optimize the predicted ratios T_B/T_A , T_D/T_C , and T_C/T_A with experimental values or values derived from interpolations of experimental trends. (b) Behavior of K_{eff} at the reference pressures p_1 and p_2 in (a). The three pressure cuts in (a) refer to the T - x phase diagrams in Figs. 22(a)–22(c).

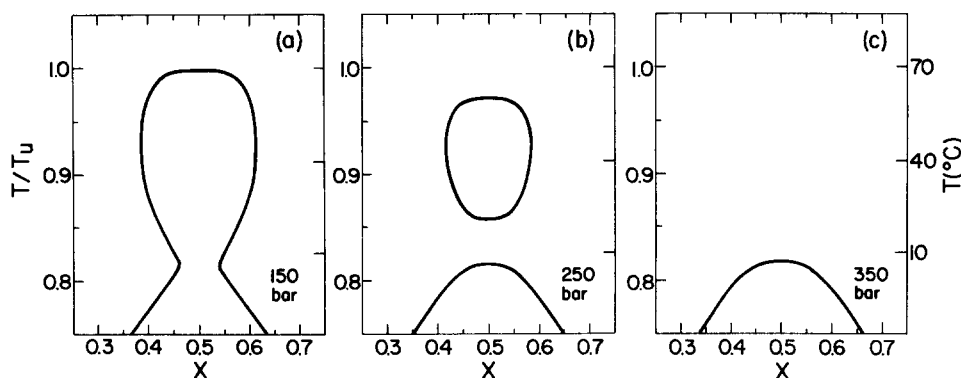


FIG. 22. Evolution of temperature-composition curves with pressure predicted for the system ethanol + H₂O + 14.40 % by weight K₂CO₃. Graphs (a), (b), and (c) correspond to pressures (i), (ii), and (iii) [150, 250, and 350 bar, respectively], in Fig. 21(a). Temperatures are normalized to the 150 bar UCST. Note the nearly constant temperature of the lowest separation as the closed loop pinches off and shrinks.

studied by a straightforward extension of the following discussion.

Figure 23 shows the experimental initial conditions in the global phase diagram for values of q and R such that the upper and lower critical solution points of the miscibility gap have merged. Therefore, while an experimental measurement is referenced to the critical temperature T_c as $|T - T_c|/T_c (= t)$, the local approach to the critical surface here is not linear but parabolic ($\propto t^2$) to leading order. Hence, the free energy, which scales like $t^{2-\alpha}$ for ordinary critical points,⁴ where α is the specific heat exponent, actually behaves as $(t^2)^{2-\alpha} = t^{4-2\alpha}$. Taking two temperature derivatives of the free energy essentially generates the specific heat,

which now scales as $t^{2-2\alpha}$. Recall that in our model this is the specific heat at constant composition $x = \frac{1}{2}$. In addition, since R and q are taken to be fixed this result also pertains to constant pressure. It is interesting to note that the specific heat is now nondivergent for $\alpha < 1$. For instance, the 3- d Ising exponent is $\sim 1/8$,³¹ giving a rounded specific heat anomaly. This result is in agreement with the work of Griffiths and Wheeler,^{45(a)} and also that of Saam,^{45(b)} with regard to the properties of a multicomponent mixture along a path of constant pressure and constant composition, in which a finite specific heat is predicted at such a special point.

This can be shown explicitly in the two-parameter model. The specific heat is as given before [Eq. (26) with $K_3 = 0$],

$$C = \left[d - \left(\frac{\partial f_I}{\partial K_I} \right) \right] \left\{ \frac{(R+1)^2 (q-1) e^{(R+1)/T}}{2T^2 [(q-1) + e^{(R+1)/T}]} \right\} + \left(\frac{\partial^2 f_I}{\partial K_I^2} \right) \left\{ \frac{(q-1) - R e^{(R+1)/T}}{2T [(q-1) + e^{(R+1)/T}]} \right\}^2. \quad (33)$$

Now, the minimum of K_{eff} occurs at a temperature T_{min} defined by the relation

$$\exp[(R+1)/T_{min}] = \frac{(q-1)}{R}. \quad (34)$$

For a small deviation δT from T_{min} , we can expand this expression and obtain

$$\exp[(R+1)/(T_{min} + \delta T)] \approx \frac{(q-1)}{R} \left\{ 1 - \ln \left[\frac{(q-1)}{R} \right] \cdot \left(\frac{\delta T}{T_{min}} \right) + \dots \right\}. \quad (35)$$

And, to leading order in $(\delta T/T_{min})$ for each term ($d=3$):

$$C \approx C_1 + C_2 \left(\frac{\partial f_I}{\partial K_I} \right) + C_3 \left(\frac{\delta T}{T_{min}} \right)^2 \left(\frac{\partial^2 f_I}{\partial K_I^2} \right), \quad (36)$$

where C_1 , C_2 , and C_3 are complicated functions of q and R alone. This explicitly shows a nonsingular background and terms proportional to $t^{1-\alpha}$ [i.e., $(\partial f_I/\partial K_I)$] and $(\delta T/T_{min})^2 \cdot t^{-\alpha}$ [i.e., $(\delta T/T_{min})^2 \cdot (\partial^2 f_I/\partial K_I^2)$]. At the critical double point formed by the merging of two critical points both the Ising energy ($\propto \partial f_I/\partial K_I$) and the Ising specific heat ($\propto \partial^2 f_I/\partial K_I^2$) have doubled exponents,

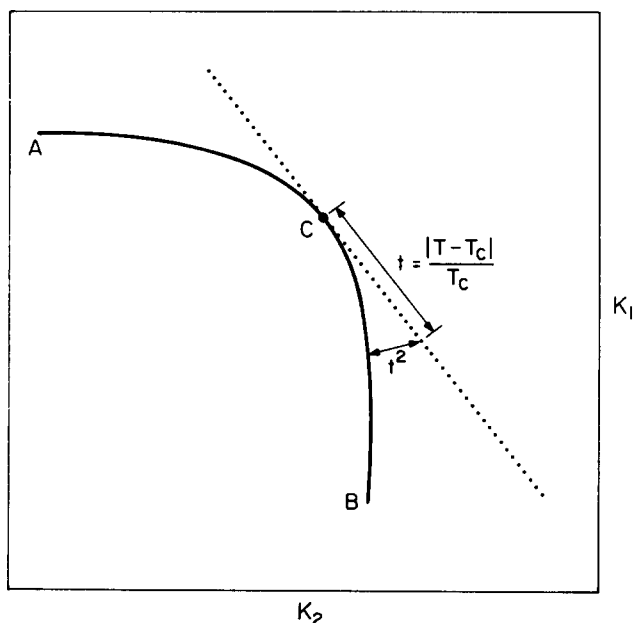


FIG. 23. Detail of temperature approach to a critical point along a path in parameter space for which renormalized critical exponents are predicted. Along the trajectory indicated by the dotted line the approach to point C is measured linearly as $t = |T - T_c|/T_c$, whereas the local approach to criticality, as measured by distance to the critical surface (line ACB), is parabolic ($\propto t^2$) to leading order.

because of the parabolic approach, but the third term has the additional factor of $(\delta T/T_{\text{min}})^2$ which is just t^2 at the critical point. Thus, the leading power law singularity is proportional to $t^{2-2\alpha}$, as pointed out above.

Note that the correlation length exponent will simply double (from ν to 2ν) in such a parabolic approach to the critical point.¹⁸ The magnetization exponent β will likewise be renormalized to 2β since the magnetization is not derived from a temperature derivative of the free energy. Experimentally, it would be difficult to verify such exponent doubling in the order parameter since the loop is vanishing at such a double point. However, as discussed in Sec. III B, there are systems, like 2-butanol + H₂O and ethanol + H₂O + K₂CO₃, which show a pinched-in miscibility curve at low pressures and a closed loop at high pressures. At some intermediate pressure, that necked-in portion of the coexistence curve should just close up, leading to the merging of the loop and a lower separation, the latter observed as distinct at higher pressures. This has been discussed by several other workers.^{25,44} This point would be characterized by a coupling constant which behaves as the lower curve in Fig. 21(b) [see also Fig. 14(b), case (iii)]. Since the loop has not vanished here, measurement of the order parameter should allow for an easy verification of exponent doubling.^{25,44} Of course, light scattering measurements could be employed equally well in either case, to determine the correlation length behavior.

Finally, we note that at these critical points, the exponent renormalization is such that the exponent scaling relations^{4,7} still hold. For example, the dimensionality d , correlation exponent ν , and specific heat exponent α are related by

$$d\nu = 2 - \alpha. \quad (37)$$

In the renormalized case (indicated by a subscript r),

$$\nu_r = 2\nu; \alpha_r = -2 + 2\alpha, \quad (38)$$

so

$$d\nu_r = 2d\nu = 4 - 2\alpha = 2 - \alpha_r. \quad (39)$$

D. Specific heat and light scattering experiments as methods of locating systems on the global phase diagrams

The methods described above for matching the parameters of these lattice-gas models to experimental data have relied upon accurate knowledge of the critical points of miscibility gaps. Yet, it has been observed in many of the real systems discussed that variation of one or more thermodynamic fields may produce a mixture which is homogeneous at all temperatures (ignoring the ever-present freezing and vaporization transitions). Systems in such a state are not precluded from study by our models: As Fig. 10 shows, even in the absence of a miscibility gap, the Ising variable nearest-neighbor correlation still exhibits a maximum as a function of temperature. This maximum occurs at the point of closest approach of K_{eff} to the Ising critical value. The locus of these maxima, as a function of R (for fixed q , as might be the case in an experiment studying the effects of electrolytes, for instance) on the global phase diagram is shown by Sec. (a) of the curve in Fig. 13.

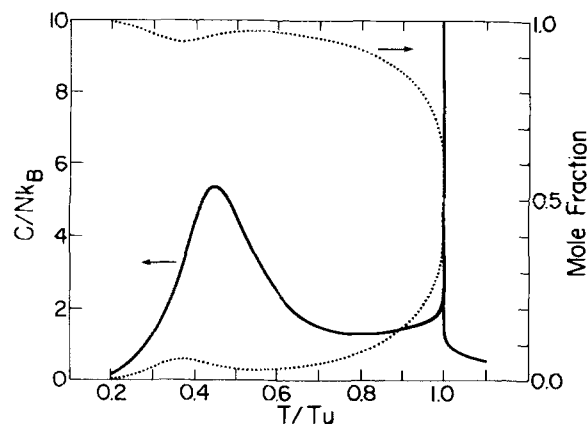


FIG. 24. Theoretical phase diagram (in T - x space) and specific heat curve for a system with a ground state of A-A and B-B but moderately strong A-B interactions. This results in a pinched-in coexistence curve and a rounded maximum in the specific heat. The system 2-butanol + H₂O at atmospheric pressure is predicted to exhibit this behavior.

Such a maximum in m correlation should be indicative of the onset of critical fluctuations and would be seen in a scattering measurement of the correlation length. Similarly, the specific heat would show a maximum along roughly the same path, although the amplitude would be small (see below) since the rise would have the high-temperature amplitude on either side. This is clear from an extrapolation of the case in Fig. 8 to beyond the merging of the LCST and the UCST. Note that as the critical point D (Fig. 13) is approached, this correlation maximum itself would saturate (as the correlation length ξ diverges), while the specific heat maxima would show a rounded approach (see Sec. III C for a discussion of critical exponent renormalization). After conditions are altered to produce a miscibility gap, the points of minimum K_{eff} , as a function of R , then represent maxima in the concentration difference between coexisting phases, and minima in the specific heat. These points correspond to Sec. (b) of the curve in Fig. 13. In essence, one can describe some of the properties of a miscible system by the same model parameters which determine the size and shape of the coexistence curve, and can follow experimental trajectories in the global phase diagrams.

Just as an approach to criticality in a homogeneous system results in the onset of long range correlations, and the associated heat capacity and scattering signals, so too does an approach from a phase separated regime. The pinched-in coexistence curves of 2-butanol and water and ethanol + H₂O + K₂CO₃ are examples relatively easily studied. Were a heat capacity measurement to be performed on such a system, the results are predicted to be like those in Fig. 24. While the specific heat diverges at the UCST, the near approach to criticality over a relatively wide temperature range, near the necked-in part of the coexistence curve, produces a broad maximum in C . Note that the peak is predicted to be shifted from the temperature of lowest concentration difference as a result of the asymmetric approach to the critical surface [see Fig. 5(a)]. This maximum is characterized by the large low-temperature specific

heat amplitudes, in contrast with the curve measured beyond the vanishing of the loop (see above).

E. More complex coexistence phenomena

The generalized Hamiltonian [Eq. (5)] has the features to describe quite a wide range of miscibility/immiscibility behavior in binary systems. However, there is no reason to expect that the interactions of many complex, multifunctional organic molecules with water or other solvents can be simplified to such a degree and still be realistic. For instance, it is clear that molecules such as glycerol, guaiacol, and hydroxyethers have multiple strongly interacting sites and form up to several discrete hydrogen bonds to neighbors in solution. Certainly, these may be of different strength and directional specificity, and interactions between neigh-

boring areas of a given molecule may be nonadditive, if charge delocalization or conformational strain is present. We have developed such a multiple-state model through the introduction of another orientational degree of freedom (another Potts-type variable μ) at each site in the lattice. For the sake of clarity we make several simplifications in the Hamiltonian in our discussion below, to demonstrate the qualitative features of this extended version of the model. First, we set the directional degrees of freedom equivalent ($\sigma_i = 1, 2, 3, \dots, q$; $\mu_i = 1, 2, 3, \dots, q$). Second, we assume that the interaction of a nearest-neighbor pair depends only on the number of bonds formed and not on which of the two possible types is involved (in the case of only one bond formed). These assumptions allow for a straightforward examination of nonadditivity of interactions. The model Hamiltonian can be written

$$-\beta\mathcal{H}_5 = \sum_{\langle ij \rangle} \{ 0\delta_{s_i s_j}(1 - \delta_{\sigma_i \sigma_j})(1 - \delta_{\mu_i \mu_j}) + K_1(1 - \delta_{s_i s_j})[\delta_{\sigma_i \sigma_j}(1 - \delta_{\mu_i \mu_j}) + \delta_{\mu_i \mu_j}(1 - \delta_{\sigma_i \sigma_j})] + K_2(1 - \delta_{s_i s_j})(1 - \delta_{\sigma_i \sigma_j})(1 - \delta_{\mu_i \mu_j}) + K_3\delta_{s_i s_j}[\delta_{\sigma_i \sigma_j}(1 - \delta_{\mu_i \mu_j}) + \delta_{\mu_i \mu_j}(1 - \delta_{\sigma_i \sigma_j})] + K_4(1 - \delta_{s_i s_j})\delta_{\sigma_i \sigma_j}\delta_{\mu_i \mu_j} + K_5\delta_{s_i s_j}\delta_{\sigma_i \sigma_j}\delta_{\mu_i \mu_j} \}, \quad (40)$$

where we have explicitly included the zero energy level to make clear the configurational rules.

A typical energy level diagram is shown in Fig. 25, with the associated particle-pair configurations. Qualitatively, one would expect this Hamiltonian to show the same properties as the basic two-parameter model [Eq. (2)] at high temperatures and repeat the pattern of mixing and demixing seen in the three-parameter model [Eq. (5)] at lower temperatures. This is so because of the relationships of the degeneracies of the pairs of energy levels ($K_2, 0$), (K_1, K_3), and (K_4, K_5). Each pair has roughly $1/q$ the degeneracy of the previous one. The energy level hierarchy in Fig. 25 will, for appropriately chosen parameters, show closed loops at both high and intermediate temperatures and a final phase separation at very low temperatures—five critical points in all. It is, of course, possible to study such a Hamiltonian using the Migdal-Kadanoff techniques employed in earlier works, or some other such approximation. However, the high dimensionality of the parameter space (at least eight dimensions with fields to determine densities) and the cumbersome configuration counting needed for the MK recursion relations make such a calculation difficult. It is in a case like this that the high-temperature series expansion used throughout this paper is extremely useful. The summation over orientational degrees of freedom [Eqs. (7)–(13)] now extends over both $\{\sigma_i\}$ and $\{\mu_i\}$, with the result (accurate to third order, as before)

$$K_{eff} = \frac{-1}{T} + \ln \left[\frac{(q-1)^2 + 2(q-1)e^{(R+1)/T} + e^{(D_1+1)/T}}{(q-1)^2 + 2(q-1)e^{S/T} + e^{D_2/T}} \right], \quad (41)$$

where, as before

$$R = -K_1/K_2, \quad (42)$$

$$S = -K_3/K_2,$$

and the double bonding energies D_1 and D_2 are

$$D_1 = -K_4/K_2, \quad (43)$$

$$D_2 = -K_5/K_2.$$

It is important to note that if the double bonding energies

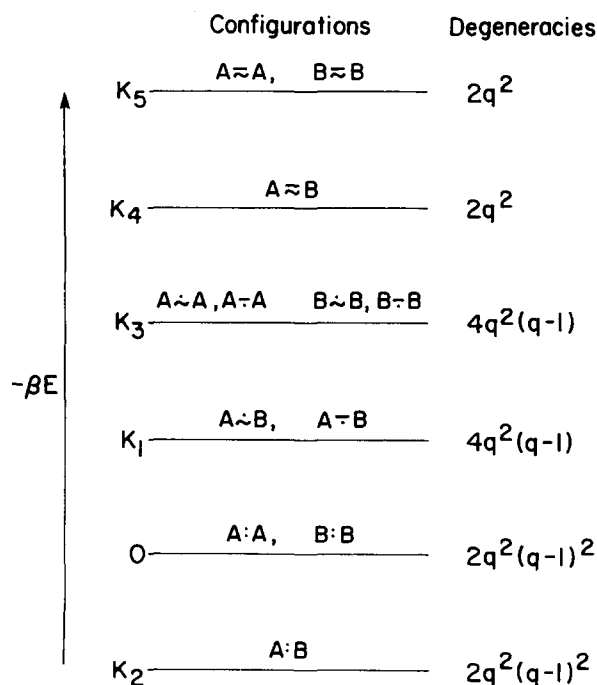


FIG. 25. Reduced-energy level diagram, configurations and degeneracies for the Hamiltonian of Eq. (40). Bonds involving only one orientational degree of freedom ($\sigma_i = \sigma_j$ or $\mu_i = \mu_j$) are indicated by \sim or \sim , while nonbonding configurations are signified by \cdot 's. Note the grouping of the energy levels into pairs with degeneracies down by a factor of roughly q from the next lowest energy pair. For appropriate spacing of a hierarchy like this, five critical points will be encountered as temperature is lowered; two closed loops and a transition to a phase separated ground state.

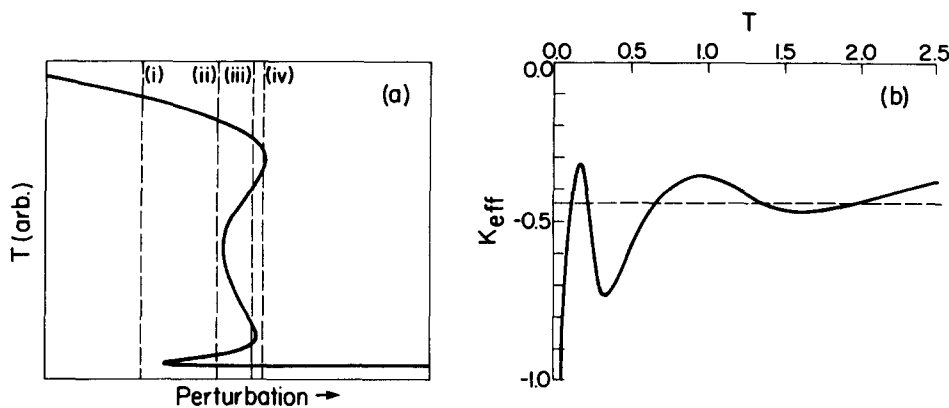


FIG. 26. (a) Evolution of critical solution points with some perturbation to the energy level hierarchy in Fig. 25. Such a perturbation might be caused by pressure or addition of a third component. For this figure, the perturbation consisted of shifting the energy level K_3 from above K_1 to below K_1 , linearly. (b) Behavior of K_{eff} with temperature [Eq. (41)], for energy levels as follows; $R = 7.2$; $S = 7.5$; $D_1 = 9.20$; and $D_2 = 9.25$. Note that the existence of an intermediate-temperature closed loop is a consequence of the very closely spaced double-bonding levels (D_1 and D_2) relative to the single-bonding spacing (between K_1 and K_3). Cross sections in (a), labeled (i)–(iv) refer to Fig. 27.

are taken to be simply additive ($D_1 = 2R$, $D_2 = 2S$), a lower closed loop is not predicted, in general: At a temperature such that the intermediate energy levels K_1 and K_3 are at the critical Ising spacing, the levels $K_4 (=2K_1)$ and $K_5 (=2K_3)$ would be at twice that spacing. Then, as temperature is further lowered, the system would fall directly into the ground state of double-bonded like nearest neighbors, without an intermediate mixed phase. Thus, the system would stay phase separated all the way down to zero temperature. A lower closed loop results from very closely spaced K_4 and K_5 energy levels.

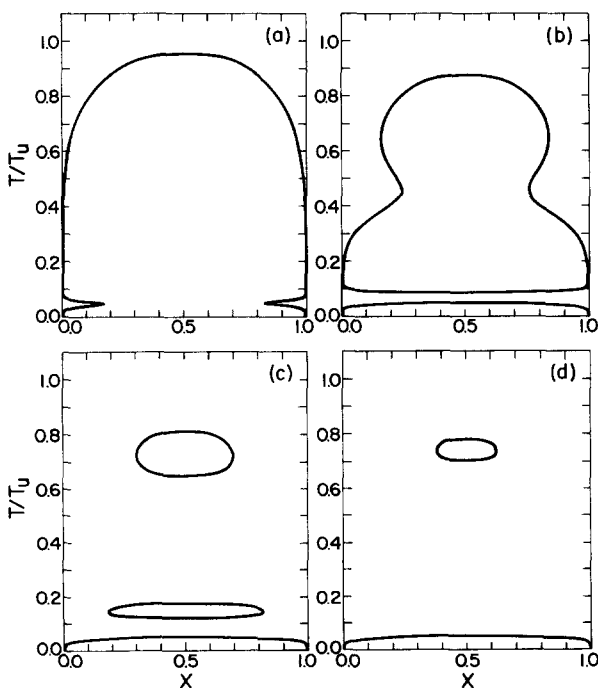


FIG. 27. T - x phase diagrams as a function of the value of the like-nearest-neighbor single-bond energy level (S), for fixed R , D_1 , and D_2 as in Fig. 26. Figures (a) through (d) refer to (i) through (iv) in Fig. 26(a).

Figure 26(a) shows the locus of critical points as the parameters are smoothly varied, while Fig. 27 shows the various phase diagrams associated with the different energy spacings. For the purpose of illustration, we have fixed all of the energies except K_3 (the single-bond like- nn energy), and linearly translated it from above to below K_1 across the figure. This corresponds to the labeled "perturbation." Also displayed [Fig. 26(b)] is the K_{eff} vs T plot for parameters such that five critical points are predicted. A full range of T - x diagrams is possible; simple phase separation, a single closed loop, a loop with a lower phase separation, two loops, and two loops with a separated ground state. Novak and Schneider¹⁴ present data on the system ethanol + H_2O + $(\text{NH}_4)_2\text{SO}_4$ (15.80% by weight) which suggests such behavior (see Fig. 28). We note, however, that one must

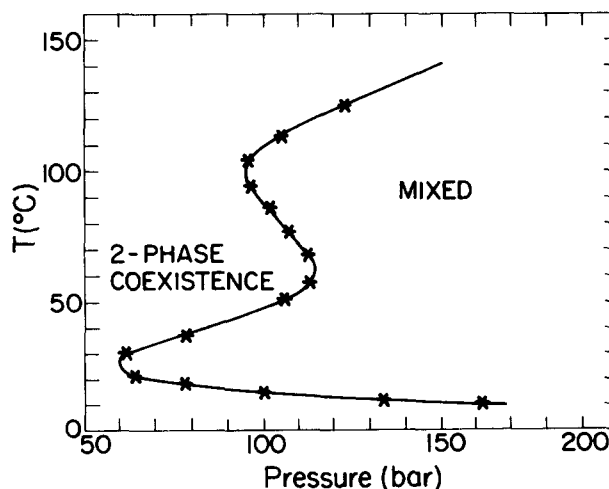


FIG. 28. Experimental data from Ref. 14 on the solution points of the system ethanol + H_2O + $(\text{NH}_4)_2\text{SO}_4$ (15.80% by weight) as a function of pressure. The curve is a guide to the eye. Note the qualitative similarity of this curve to that in Fig. 26. The absence of a high temperature UCST may be due to a pre-emptive vaporization.

exercise caution in making such an identification. For example, these experiments are carried out at constant composition, thus the data points shown in Fig. 28 indicate only where phase separation occurs and are not in general critical points. The fact that a homologous series of such results is obtained for different concentrations of $(\text{NH}_4)_2\text{SO}_4$ strengthens the interpretation that the critical points also display this behavior, but certainly, more complete experimental results on such a system would be of great interest. The highest solution temperature is not indicated in Fig. 28 and was either outside the experimental range or preempted by a vaporization transition. Finally, it is interesting to note that the sulfate ion is a coordinating species which can be either monodentate or bidentate,⁴⁶ and in the high concentration in these mixtures, it may provide a multiple bonding mechanism as a bridging coordinated species between the major components.

As before, a more detailed microscopic description of the nature of the interactions is needed before conclusions can be drawn about the various parameters' trends in fitting experimental data.

F. Symmetry-breaking interactions

As pointed out previously, it is observed experimentally that most binary mixtures, especially aqueous systems, show $T-x$ phase diagrams in which the coexistence curves are asymmetric with respect to mole fraction 1/2. While some of the asymmetry is due to size effects, it is clear that asymmetries in like-neighbor interactions play a role. For instance, in the system studied by Cox,¹⁵ the pyridine-pyridine interactions are clearly weaker than the $\text{D}_2\text{O}-\text{D}_2\text{O}$ interactions. The decorated models^{24(b)} have been successful in taking such effects into account. Our generalized model^{6,7} can also be extended to account for this by the introduction of an interaction between bonded species of the form

$$\sum_{\langle ij \rangle} \frac{h_1}{2d} (s_i + s_j) \delta_{\sigma_i \sigma_j}, \quad (44)$$

where the factor $1/2d$ has been included because there are $2d$ bonds per site on a hypercubic lattice (this is simply a "book-keeping" detail). The interaction splits the degeneracy of the K_3 energy level (see Fig. 1) such that an AA (++) bonded pair has energy $K_3 + h_1/d$, while a BB (--) pair has a less favorable energy $K_3 - h_1/d$ (for $h_1 > 0$). We are currently studying this extra term in various approximations, including PSRG and the high-temperature series expansion. Results will be reported in a forthcoming work.⁴⁷

IV. CONCLUSIONS

We have shown that the experimental phase diagrams of a number of binary mixtures of complex organic molecules, and aqueous solutions, can be located, often quantitatively, in the global parameter space of several lattice-gas Hamiltonians. Methods for performing these mappings have been developed based on the trends in the critical solution temperatures as a function of some system perturbation, such as pressure. In several cases,

especially isotopic substitution experiments (on the system 3-methyl pyridine + $\text{H}_2\text{O}/\text{D}_2\text{O}$) and electrolyte and dilute third component addition, the observed trends in the theoretical parameters are in accord with a specific microscopic picture of the intermolecular interactions.

A number of binary mixtures show evidence for the existence of special critical points at which critical singularities are predicted to have renormalized exponents. These systems are often easily accessible to experiments in that these points lie at temperatures and pressures not far removed from ambient conditions. Experimental work on heat capacity, order parameter and correlation length exponents would be extremely illuminating of the issue of exponent changes. We have also shown how nonseparating mixtures can be characterized in terms of the parameters of the models.

The high-temperature series expansion used in this work makes complex lattice-gas Hamiltonians of the type used here easy to study. The results are in close agreement with more complex PSRG calculations. In particular, the use of continuously varying orientational interactions, instead of the discrete ones used here, may be a useful path to explore.

Finally, we note that the introduction of thermodynamic vacancies into these lattice-gas models allows for the study of the liquid-vapor transition, which is of relevance to a wide variety of industrial processes and theoretical studies. Work is currently progressing on such studies and will be reported in a forthcoming work.⁴⁸

ACKNOWLEDGMENTS

We thank John C. Wheeler for a careful reading of the manuscript and many helpful suggestions. We also thank A. N. Berker for his comments and a reading of the work. Finally, we have profited from enlightening discussions with David Chandler on the properties of water and aqueous solutions, and from numerous discussions with Chester A. Vause. R.E.G. acknowledges support from the Northeast Division of the American Chemical Society through a James Flack Norris Undergraduate Research Fellowship. This work was supported by NSF under Grant No. DMR81-19295.

¹J. S. Rowlinson, *Liquids and Liquid Mixtures*, 2nd ed. (Plenum, New York, 1969).

²A. W. Francis, *Liquid-Liquid Equilibrium* (Wiley, New York, 1963).

³*Phase Transitions and Critical Phenomena*, edited by C. Domb and M. S. Green (Academic, New York, 1972), Vols. 1-6; L. D. Landau and E. M. Lifshitz, *Statistical Physics*, 2nd ed. (Pergamon, Oxford, 1969).

⁴*Introduction to Phase Transitions and Critical Phenomena* (Oxford University, Oxford, 1971).

⁵J. S. Walker and C. A. Vause, *Phys. Lett. A* **79**, 421 (1980).

⁶J. S. Walker and C. A. Vause, in *Eighth Symposium on Thermophysical Properties*, edited by J. V. Sengers (American Society of Mechanical Engineers, New York, 1982), Vol. 1, pp. 411-418.

⁷J. S. Walker and C. A. Vause (preprint).

⁸C. A. Vause and J. S. Walker, *Phys. Lett. A* **90**, 419 (1982).

- ⁹J. D. Hirschfelder, D. Stevenson, and H. Eyring, *J. Chem. Phys.* **5**, 896 (1937).
- ¹⁰G. Schneider, *Z. Phys. Chem. (Frankfurt am Main)* **39**, 187 (1963).
- ¹¹G. Schneider, *Adv. Chem. Phys.* **17**, 1 (1970).
- ¹²In addition to simple miscibility domes, many systems show de-mixing phenomena again at very high pressures (several kbar). See, for instance, G. Schneider, *Ber. Bunsenges. Phys. Chem.* **70**, 497 (1966).
- ¹³G. Schneider and C. Russo, *Ber. Bunsenges. Phys. Chem.* **70**, 1008 (1966).
- ¹⁴J. P. Novak and G. M. Schneider, *Ber. Bunsenges. Phys. Chem.* **72**, 791 (1968).
- ¹⁵J. D. Cox, *J. Chem. Soc.* **1952**, 4606.
- ¹⁶B. A. Scheibner, M. R. Meadows, R. C. Mockler, and W. J. O'Sullivan, *Phys. Rev. Lett.* **43**, 590 (1979).
- ¹⁷A. Deerenberg, J. A. Schouten, and N. J. Trappeniers, *Physica* **103**, 183 (1980).
- ¹⁸A. R. Kortan, N. H. Känel, R. J. Birgeneau, and J. D. Litster, *Phys. Rev. Lett.* **47**, 1206 (1981).
- ¹⁹E. Bloemen, J. Thoen, and M. Van Dael, *J. Chem. Phys.* **73**, 4628 (1980).
- ²⁰An extensive treatment of binary system phase equilibrium for van der Waals mixtures is given in P. H. van Konynenburg and R. L. Scott, *Philos. Trans. R. Soc. London*, **298**, 495 (1980).
- ²¹Examples of calculations of binary mixture properties using Lennard-Jones type intermolecular potentials along with multipole expansions of angular interactions can be found in K. E. Gubbins and C. H. Twu, *Chem. Eng. Sci.* **33**, 863 (1978); C. H. Twu and K. E. Gubbins, *Eng. Sci.* **33**, 870 (1978).
- ²²J. A. Barker and W. Fock, *Discuss. Faraday Soc.* **15**, 188 (1953).
- ²³J. C. Wheeler, *J. Chem. Phys.* **62**, 433 (1975).
- ²⁴(a) G. R. Anderson and J. C. Wheeler, *J. Chem. Phys.* **69**, 2082 (1978); (b) *ibid.* **69**, 3403 (1978).
- ²⁵J. C. Wheeler and G. R. Anderson, *J. Chem. Phys.* **73**, 5778 (1980).
- ²⁶J. C. Wheeler, *Annu. Rev. Phys. Chem.* **28**, 411 (1977).
- ²⁷A. A. Migdal, *Sov. Phys. JETP* **42**, 743 (1976).
- ²⁸L. P. Kadanoff, *Ann. Phys.* **100**, 359 (1976).
- ²⁹H. Chou, B.S. thesis, M.I.T., 1981.
- ³⁰D. A. Seibert, B.S. thesis, M.I.T., 1981.
- ³¹We have used the Padé approximants to the 3-d Ising ferromagnet thermodynamic properties given in P. E. Scesney, *Phys. Rev. B* **1**, 2274 (1970).
- ³²A low-temperature series expansion for the properties of the 3-d Ising ferromagnet can be found in M. F. Sykes, J. W. Essam, and D. S. Gaunt, *J. Math. Phys. (N. Y.)* **6**, 283 (1965).
- ³³A high-temperature series approximation for the 3-d Ising ferromagnet is in C. Domb, *Adv. Phys.* **9**, 149 (1960).
- ³⁴R. B. Potts, *Proc. Cambridge Philos. Soc.* **48**, 106 (1952).
- ³⁵F. Y. Wu, *Rev. Mod. Phys.* **54**, 235 (1982).
- ³⁶R. G. Johnston, M. R. Meadows, R. C. Mockler, and W. J. O'Sullivan (preprint, 1982). In this method, the mole fraction x is transformed into the variable ϕ via
- $$\phi = \frac{x}{x + p(1-x)},$$
- with the requirement that when $x = x_c$ (the upper or lower critical solution point concentration) the value of ϕ is 1/2. This determines p to be $x_c/(1-x_c)$. See also Ref. 24(a) for the use of data symmetrization methods.
- ³⁷T. Moriyoshi, S. Kaneshina, K. Aihara, and K. Yabumoto, *J. Chem. Thermodyn.* **7**, 537 (1975).
- ³⁸W. Dolgolenko, *Z. Phys. K. Chem.* **62**, 499 (1908).
- ³⁹G. Poppe, *Bull. Soc. Chim. Belg.* **44**, 640 (1935).
- ⁴⁰B. C. McEwan, *J. Chem. Soc.* **123**, 2284 (1923).
- ⁴¹J. C. Wheeler (private communication).
- ⁴²G. C. Pimentel and A. L. McClellan, *The Hydrogen Bond* (Freeman, New York, 1960).
- ⁴³*Hydrogen-Bonded Solvent Systems*, Proceedings of a Symposium on Equilibria and Reaction Kinetics in Hydrogen-Bonded Solvent Systems, edited by A. K. Covington and P. Jones (Taylor and Francis, London, 1968).
- ⁴⁴J. T. Bartis and C. K. Hall, *Physica* **78**, 1 (1974).
- ⁴⁵(a) R. B. Griffiths and J. C. Wheeler, *Phys. Rev. A* **2**, 1047 (1970); (b) W. F. Saam, *ibid.* 1461 (1970).
- ⁴⁶F. A. Cotton and G. Wilkinson, *Advanced Inorganic Chemistry*, 3rd ed. (Wiley, New York, 1972), p. 641.
- ⁴⁷R. E. Goldstein and J. S. Walker (to be published).
- ⁴⁸R. G. Caflisch and J. S. Walker (to be published).